Selenology Today

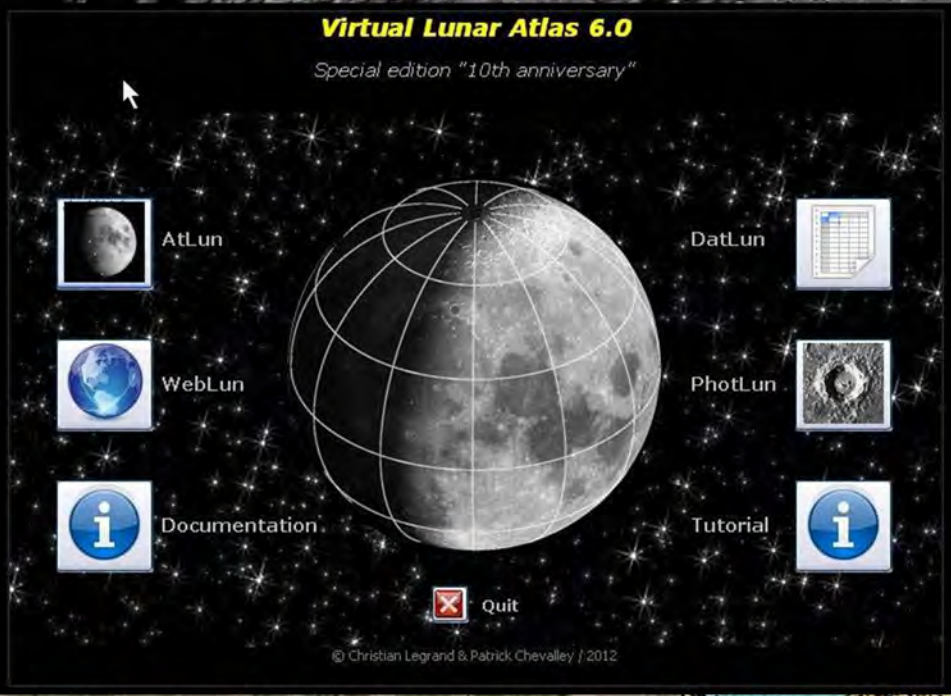

ISSUE # 31, 2013

Selenology Today

Selenology Today is devoted to the publication of contributions in the field of lunar studies. Manuscripts reporting the results of new research concerning the astronomy, geology, physics, chemistry and other scientific aspects of Earth's Moon are welcome. Selenology Today publishes papers devoted exclusively to the Moon. Reviews, historical papers and manuscripts describing observing or spacecraft instrumentation are considered.

Selenology Today website

http://digilander.libero.it/glrgroup/

and here you can found all older issues

http://www.lunar-captures.com/SelenologyToday.html

In this issue of Selenology Today not only Moon
(see the contents in following page).

Selenology Today is under a reorganization, so that further comments sent to us will help for the new structure. So please doesn't exit to contact us for any ideas and suggestion about the Journal. Comments and suggestions can be sent to Raffaello Lena editor in chief : gibbidomine@libero.it

ISSUE # 31, 2013

Selenology Today

Contents

COVER

- South Pole
by George Tarsoudis

- Screen Shoots from VMA

- Partial Solar Eclipse
by Maurice Collins

Selenology Today

Virtual Moon Atlas

10th anniversary / Pro 6" version

by Christian Legrand and Patrick Chevalley

I'm happy, with Patrick Chevalley, to announce you that we have just released the new Virtual Moon Atlas "10th anniversary / Pro 6" version !
In 2002 we published the first version of the VMA. Today, for its 10th anniversary, we are happy to present you the new Pro 6 version, the most complete computerized lunar atlas.
Since December 2009, release date of the Pro version 5, we were waiting the datas sent by the recent lunar probes US LRO and chinese Chang'e 2 so that we could format them for use in VMA. It's now done and we also fill this gap period in our production to add new modules and functionalities. We have also update and increase the databases. We hope that all this new work will make lunar observing sessions still more interesting.
And we can't not forget to dedicate this new version to Neil Armstrong whose "small step and giant leap" have conducted many of us to become amateur astronomers and specially lunar observers.
We will now present you all the news of this version that spread us in the new 10 years coming :

THE NEW "COMMAND CENTER"
Because of the increasing number of modules in VMA Pro version, VMA is launched now from a "Command Center" that gives you a direct access to each module and to the associated documentations.

THE NEW "WEBLUN" (c) MODULE :
We have realized a new special database about the main Web sites dedicated to Moon exploration and lunar surveys.
- General sites
- Lunar atlases
- Lunar probes
- Apollo missions
- Lunar observers associations
- Amateurs lunar pictures
- On line lunar ebooks
- Others lunar sites

The new "WEBLUN" (c) module manages a quick access to these sites. So, if your computer has a WiFi access during your observing sessions, you will be able to consult these sites directly from VMA while observing.

THE UPGRADES OF THE "ATLUN" (c) MODULE
- Upgrade of the terminator dynamic shadows with LRO datas
- New CCD cameras field visualization on the map
- New altazimutal and "Dobson" telescopes dedicated lunar globe orientation

THE NEW "LRO / Lunar Reconnaissance Orbiter" HIGH RESOLUTION TEXTURE :
We propose you a new texture corresponding to the best released datas of Lunar Reconnaissance Orbiter probe. It reaches 100 m resolution per pixel. We are waiting a new more precise release in the following monthes. This texure is linked to the new IAU lunar nomeclature.

THE NEW "CE2 / Chang'E 2" TEXTURE :
Chines authorities have released on 2012 february a global lunar map with a 60 m resolution per pixel. We have built a new texture comparable to the LOPAM texture yet available, but with an almost vertical lighting.

Selenology Today

THE 5 NEW "HISTORICAL TEXTURES" :
We have formatted for VMA the best digitized versions of old lunar maps in the public domain. You can know compare these pioneering works with today datas. These maps, sure, only show the visible face and the formations positions are sometimes far from the actual one. We propose you the following maps :
- Langenus / 1645 (Version : N & B)
- Hevelius / 1647 (Version : N & B & color)
- Cassini / 1676 (Version : N & B)
- Tobias Mayer / 1775 (Version : N & B)

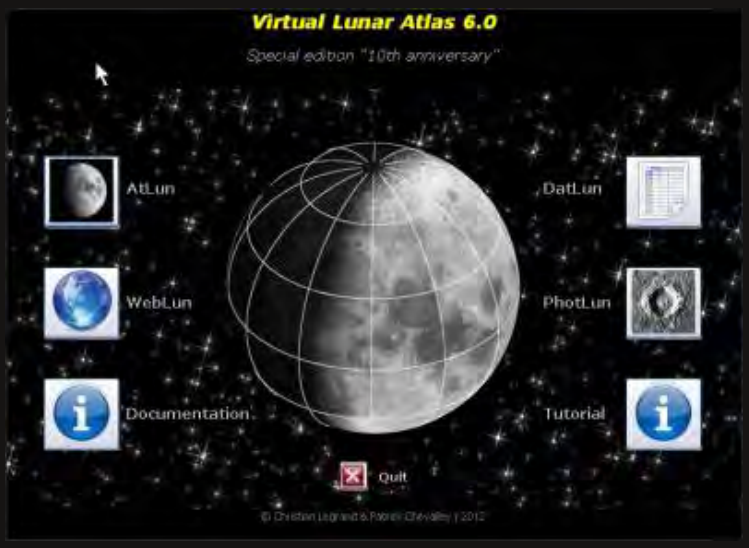

5 NEW SCIENTIFIC OVERLAYS :
- LRO Surface roughness (Surface roughness according to Lunar Reconnaissance Orbiter datas)
- LRO Surface slope and roughness (Surface slope & roughness according to Lunar Reconnaissance Orbiter datas)
- LRO Silicates (Surface silicates amount according to Lunar Reconnaissance Orbiter datas)
- Chang'e Daytime surface temperature (Surface temperature during lunar day time according to Chang'e 1 datas)
- Chang'e Nighttime surface temperature (Surface temperature during lunar night time according to Chang'e 1 datas)

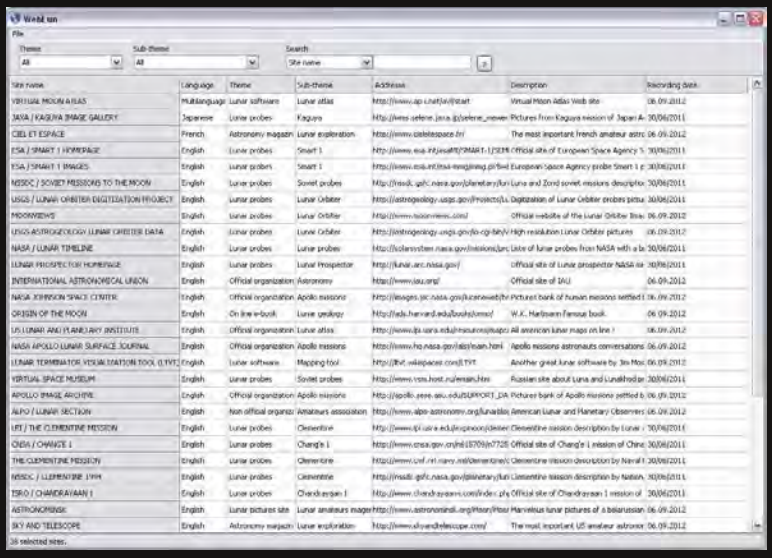

THE INTEGRATION OF NEW INTERNATIONAL ASTRONOMICAL UNION NOMENCLATURE
Jennifer Blue and her team have revised the IAU lunar nomenclature with the LRO datas. We have also revised the VMA databases to incorporate this new IAU lunar nomenclature and to correct an important number of initial mistakes.

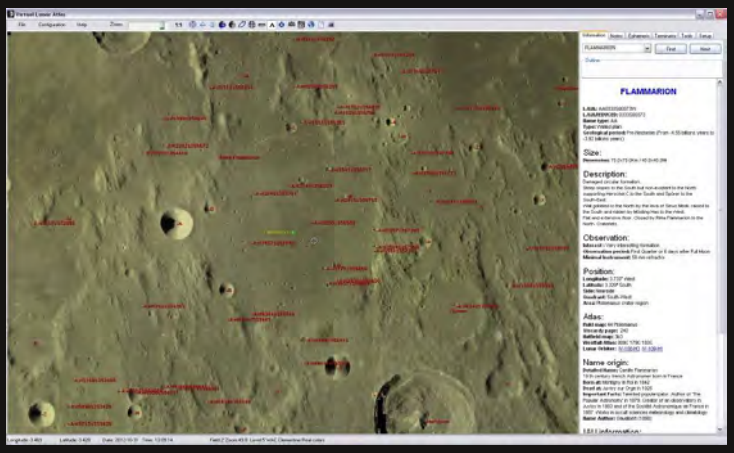

THE NEW "ANONYMS CRATERS" DATABASE
The fifth VMA database presents 52 000 anonyms craters compiled by G. Salamunićcar, S. Lončarić and E. Mazarico. Thanks to them for their permission to use their work in VMA. With this addition, VMA contains now more than 60 000 formations references.

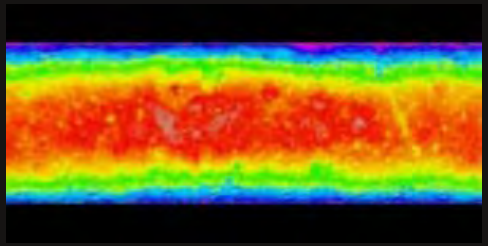

THE CONCEPTION AND INTEGRATION OF THE "LUN / Lunar Universal Number" (c) Because of the presence of formations without an official IAU name in the VMA global database, Christian Legrand has conceived the "LUN / Lunar Universal Number"

(c) that permits to localise in an unique way every lunar formation more than 10 m large. As it's unique for each lunar formation and as everybody can built easily the LUN of each formation, it becomes a very powerful tool for future recognizition of anonymous formation and discussions on them. This VMA exclusive field is now incorporated in every VMA databases.

THE NEW PICTURES LIBRARY "T1M PDM / 1 meter telescope of Pic du Midi" :
We have extracted pictures taken by a french team with the 1 meter telescope of Pic du Midi observatory (JL Dauvergne, P. Tosi, E. Rousset, F. Colas, C. Villadrich,et T. Legault) which are the best lunar pictures ever taken from the Earth surface. Really amazing. Thanks to the team to allow us in using their production.

THE NEW PICTURES LIBRARY "Best of Peach" :
Damian Peach is one of the best world lunar imager. He gives us authorization to buit a "Best of Peach" pictures libray with his production for supporting VMA. Damian has produced one of the most detailed and most numerous set of lunar formations and it's a very important addition to the software. Thanks to him !

THE NEW DOCUMENTATION :
The general documentation of VMA PRO 6.0 has been updated with new screen captures and pictures showing the new abilities of this version 6.

THE NEW VMA DVD
As the amount of datas included in VMA has grown considerably with the new HR textures, we now distribute a complete version on a DVD for people whose Internet connection is too slow for reliable downloads.

We invite you to download freely and test this new version.

http://ap-i.net/avl/en/start

Report on the Partial Solar Eclipse 2012 Nov 14.

By Maurice Collins

The day dawned cloudy but promising, with some breaks and remained so for most of the day with 7/8 cloud, but there were many thin patches and breaks so sun visible off and on throughout the morning.

For viewing the eclipse I used a 60mm refractor with 22mm eyepiece in solar projection mode. I also viewed the solar eclipse with "eclipse/transit of Venus" solar glasses to get a nice view with naked eye. All times are NZ daylight savings time, which is 13 hours ahead of UT. Since the times are variable on location, it is easier to report the times in local time. For help in converting, the Universal Time (UT) of first contact was Nov 13, 20:25UT.

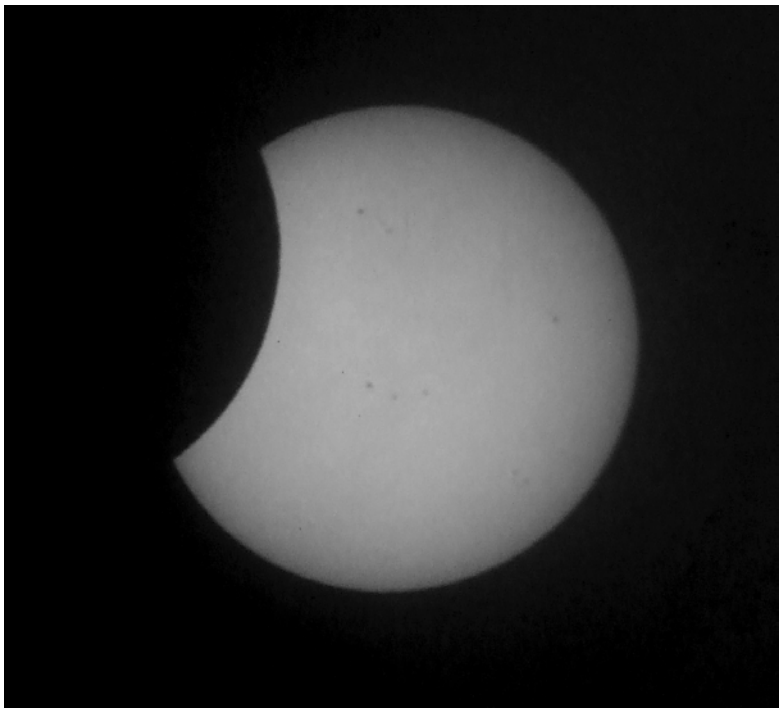

Fig 2. Eclipse at 9:41am

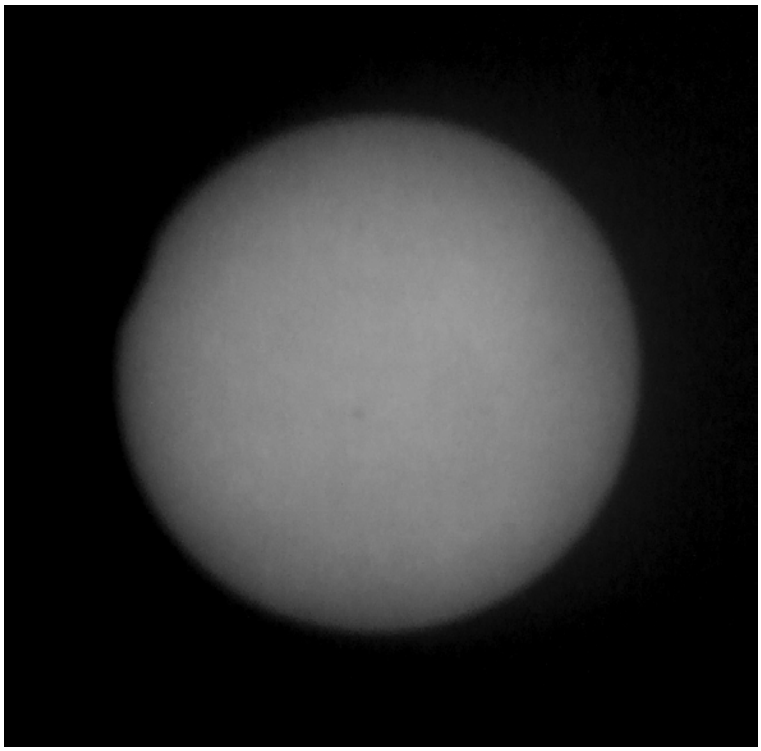

Fig 1 Shortly after first contact, 9:26am NZDT

The solar eclipse started here in Palmerston North, New Zealand at 9:25am with the sun at an altitude of 39 degrees. I saw the first contact, or just a few seconds after it was noticeable, when the limb of the sun showed the dent of the leading edge of the Moon, which was moving rapidly onto the suns disk. Clouds remained intermittent and got periodic views and images as seen below.

As the eclipse progressed the temperature seemed to drop and the wind increased, as did the cloud cover and I had to put on a jacket as it was quite icy.

But near middle of the eclipse period at from 10:00am to 10:33am there were many breaks in the cloud and the temperature warmed considerably. The sky was not noticeably darkened, about same as would be expected by the cloud cover and no apparent twilight effect as I have observed in past eclipses on clear sky days. Right around mid-eclipse, it was quite cloudy with a solar halo visible.

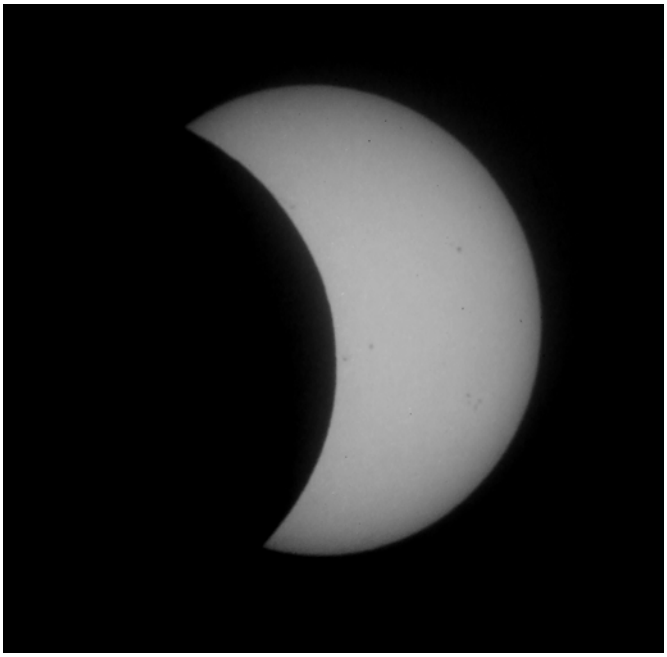

Fig 3 Eclipse at 10:00am

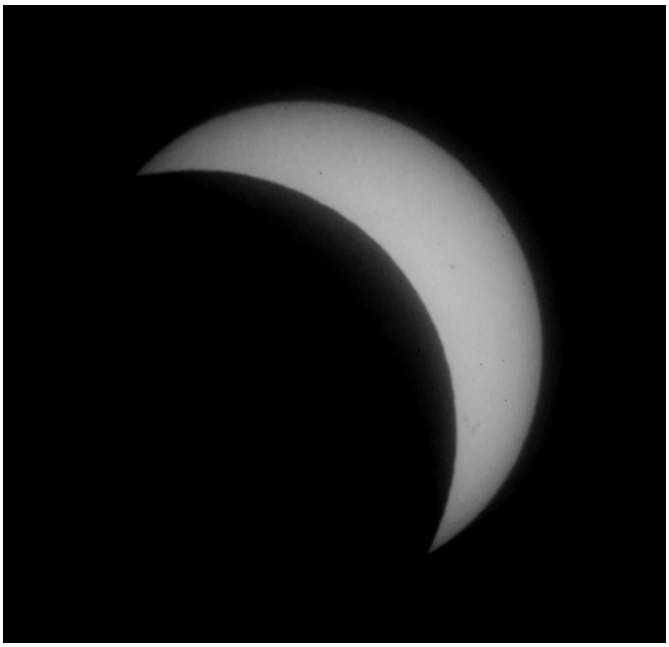

Fig 4 Eclipse at 10:21am

Shortly after mid eclipse my retired neighbour came out into his garden and I passed the solar glasses over the fence to him to see it. It was the first time he had seen an eclipse in all his years and was quite amazed by it!

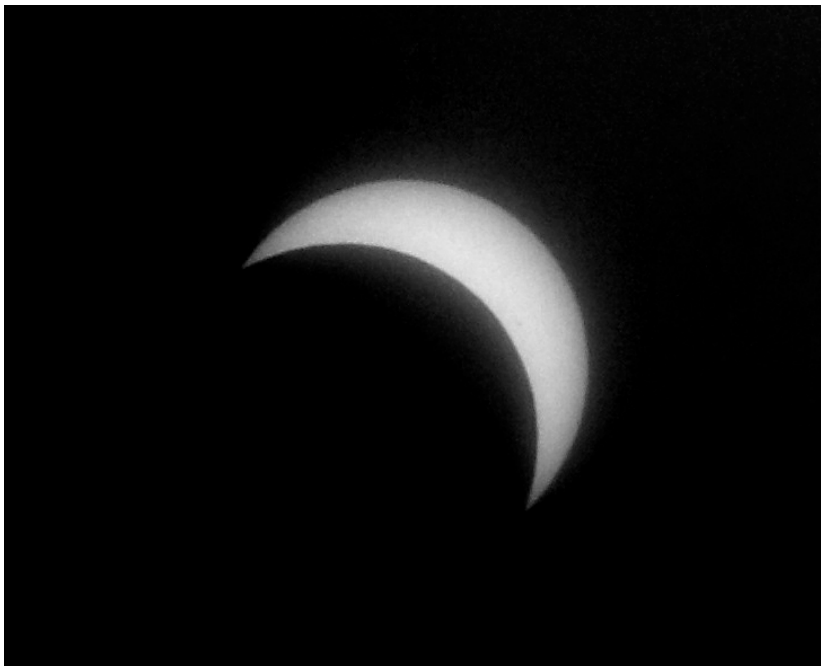

Fig 5 Best image nearest mid-eclipse, this taken shortly before at 10:27am.

Mid-eclipse was at 10:33am with the Sun at 51 degrees altitude, and the Sun was 79.5% covered by the Moon. Several small sunspots were visible, but the thin and intermittent cloud prevented and details of sunspot occultation's being observed.

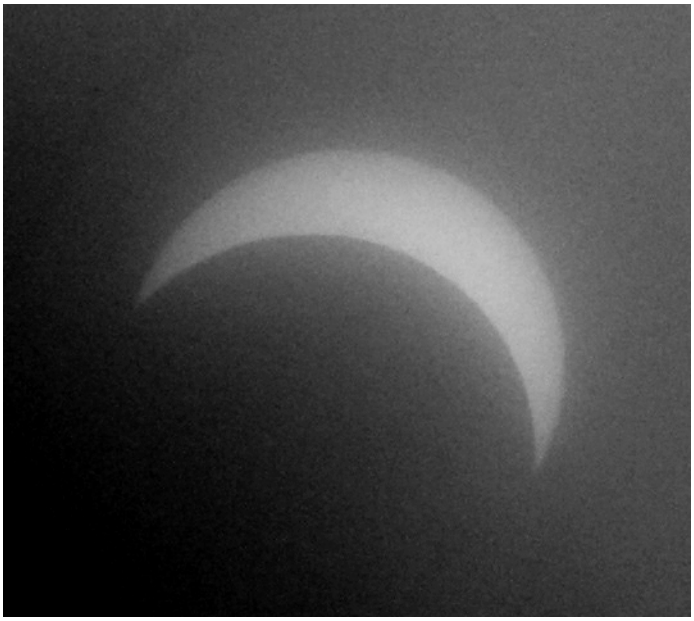

Fig 6 View through thin cloud at mid-eclipse

Fig 7 Clouds at mid-eclipse with halo.

The solar eclipse was total for northern Australia and in the Pacific ocean north of New Zealand.

The retreat of the Eclipse was in more cloud which became quite solid near the end, but I observed it a few times but as not as concerned as it was a reverse of the ingress. The eclipse ended at 11:44am and I saw some naked eye views of the Moon near the limb shortly before final contact.

Fig 8 Retreat of Moon at 11:08am

Fig 9 60mm Telescope setup used for eclipse.

It as good to see it as the weather could have been much worse and I got to see all the major parts of the eclipse and some where the clouds totally parted so the sun was in the clear for photography of it. Once again my wife was away and missed it (she was in Hobart, Tasmainia, Australia) and my daughter was at sports day at school, and did not see it either. But they enjoyed seeing the images.

ISSUE # 31, 2013

Selenology Today

Five probably meteoroids impact on the Moon

Marco Iten (a), Raffaello Lena (b), Stefano Sposetti (c)
(a) Garden Observatory

Abstract

We report the detection of five probable meteoroidal impacts on the lunar surface during post-new Moon periods. These detections were all made in year 2012. These flashes were simultaneously recorded by two or three telescopes equipped with videocams. The instruments were separated by some kilometers. Most flashes were brief. Three events correspond probably to sporadic meteoroids. For two of them, we could estimate a peak brightness and compute that the probable size of the meteoroids are likely to range about 3-12 cm and producing small craters of about 2-7 m.

1. Instruments and observing methods

Our equipment and observing procedure was presented and discussed in preceding reports (i.e. Sposetti et al., 2011; Lena et al., 2011) published in Selenology Today N. 23, 24 and 25.

We observe with different telescopes from different locations:
- a 125mm refractor, located in Gordola, Switzerland.
- a 200mm, 280mm and 420mm reflectors located in Gnosca or in Bellinzona, Switzerland.

The instruments are equipped with Watec 902H2 Ultimate and Watec 902H2 Supreme videocameras. Some GPS time inserters (KIWI-OSD and IOTA-VTI) print the Universal Time with millisecond precision in the video frames. Time synchronicity of the recorded files is therefore assured.

2. Detections

Table 1 shows all important informations about the detections. Some of them were made using ©: http://ssd.jpl.nasa.gov/horizons.cgi

We could evaluate the maximum luminosity of the events only in some cases. The absence of stars and the presence of only a couple of them in different times windows is the major obstacle for a correct evaluation of the light intensity emitted by the events.

The luminosity intensity of event N.5 was quite high and in both recordings the signal was saturated. We checked for artificial satellites in the field of views with © www.calsky.com. No satellites were on the line of sight.

We calculated the parallax angle of the Moon as seen from the Observing Site 1 and 2. This was made for an evaluation of the parallax angle of a typical geostationary satellite. The lowest parallax angle was 6.9arcsec (event N.5). A typical geostationary satellite in the line-of-sight, it subtend a parallax angle of 40 arcsec, ie. a separation of 14 pixels (Marco Iten's setup has a resolution of 2.8arcsec/pixel, see Selenology Today N. 23). In the case of event N.5 the matching between the position of the flashes in the two images is identical.

3. Active Meteor Showers

The dates of the events N.1, N.2 and N.3 are not associated with any important shower. Accordingly to the International Meteor Organization (www.imo.net/calendar/2012) when the flash N.4 happened, the Leonids (maximum the November 17, 09h30m UT, ZHR = 15?) and the α–Monocerotids (maximum the November 21, 09h55m UT, ZHR=variable) were active. When the flash N. 5 happened , the Geminids (maximum the December 13, 23h30m UT, ZHR=120) and the Comae Berenicids (maximum the December 15, ZHR=3) were active.

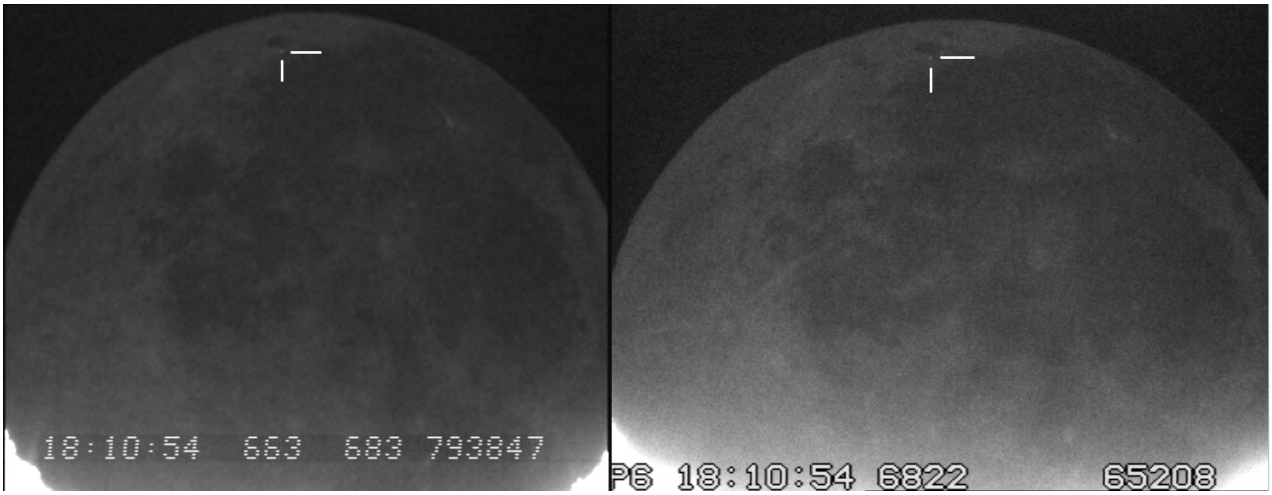

Image 1A. Event N.1 of the Feb 26 2012.

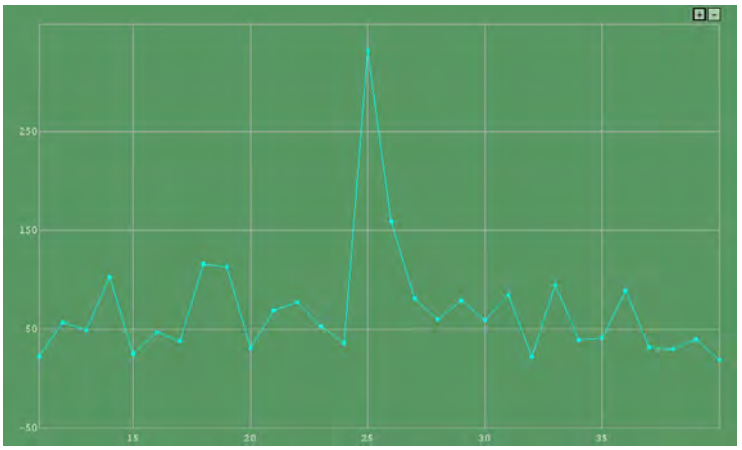

Image 1B. Lightcurve of the event N.1 of the Feb 26

4. Size of the probable impactors and of their produced craters

We assume a typical sporadic impactor speed for the (brightness) measurable events N.2 and N.3. According to the statistics of a large meteoroid orbit database (Steel, 1996) the speed for sporadic meteoroid is approximately 20.2 km s^{-1} on Earth and 16.9 km s^{-1} on the Moon, after correcting for the different escape velocities of the Earth and the Moon. It should be noted, however, that these values are nominal, since the results includes uncertainties in projectile density, meteoroid mass and luminous efficiency.

Using the luminous efficiency $\eta = 2 \times 10^{-2}$ (Ortiz et al., 2002) the masses of the impactor would be 0.103 kg and 0.052 Kg for events N. 2 and N. 3, respectively. The uncertainties in the impactor masses (from 0.041 kg to 0.258 kg for event N.2 and from 0.020 kg to 0.130 kg for the event N.3) arise from the uncertainties in the peak brightness estimate (9.3 ± 1 and 9.6 ± 1 Mag V). Based on the above data and assuming a spherical projectile, the diameter of the impactor was inferred to be approximately of about 7 cm and about 4 cm for events N.2 and N.3 respectively. Using Gault's scaling law in regolith for crater sizes, the size of the lunar impact crater was computed to be 1.9-3.0 m for the event N.2. These values are similar for different impact angles of the meteoroids. Using the Piscaled law for transient craters, the final crater is a simple crater with a rim-to-rim diameters of about 3.4 m for first brightness event, while it is inferred to be about 2.0 m for flash originated by event N.3 . The impactor would strike the targets with an estimated average energy of about 1.65 x 10^7 Joules.

If we assume a luminous efficiency of $\eta = 2 \times 10^{-3}$ the computation yields a higher average energy by a factor of 10. Moreover a luminous efficiency of 2×10^{-3} yields a mass of the impactors considerably higher than the preceding inferred value by a factor of 10. In this case, assuming the same parameters as those used in the previous computations, the impact flash N.2 appears to have been produced by a body with diameter of approximately 10 cm when assuming a spherical projectile, originating a final crater with diameters of 4-6 m (the upper and lower limit inferred taking into account the uncertainties in the peak brightness estimate). Using the luminous efficiency $\eta = 2 \times 10^{-3}$ the mass of the impactor of the second event, corresponding to flash N. 3, amounts to 0.52 kg, with uncertainties in the impactor masses (from 0.20 kg to 1.3 kg). Also in this case, using Gault's scaling law in regolith for crater sizes, the size of the lunar impact craters for the event N.3 were computed to be comprised from 2.9 m - 4.8 m.

Selenology Today

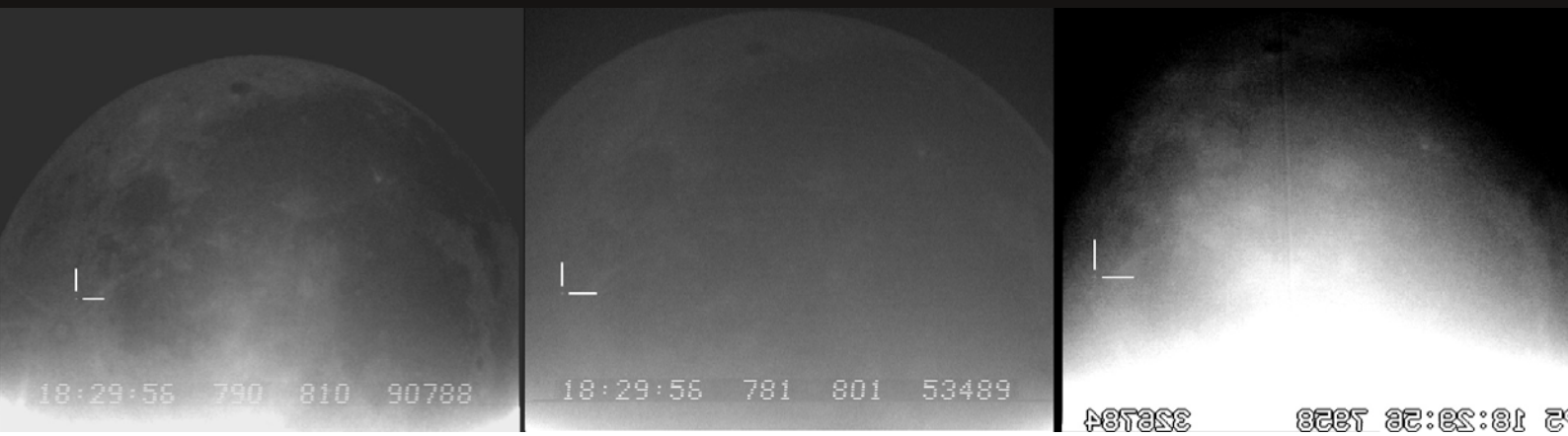

Image 2A. Event N.2 of the Mar 28 2012

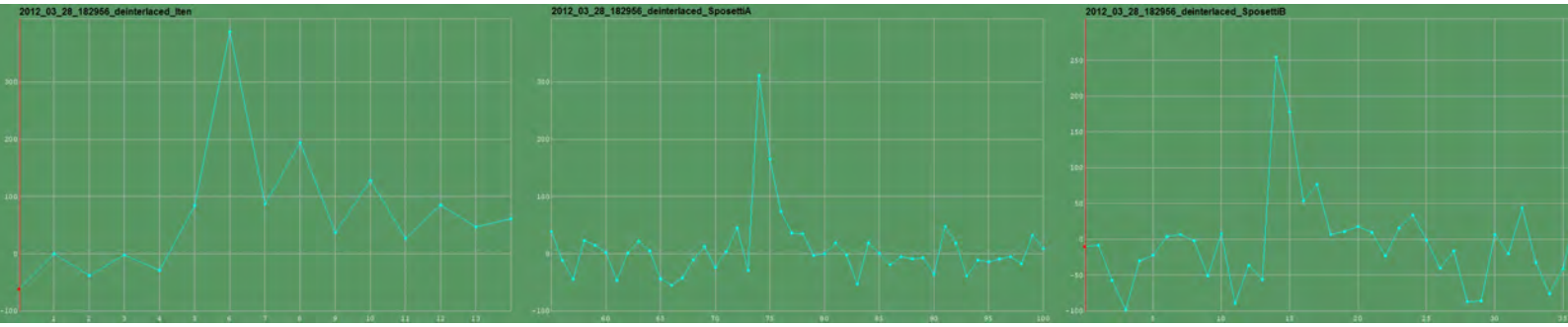

Image 2B. Lightcurves of the event N.2 of the Mar 28 2012

Image 3A.
Event N.3 of the Mar 28 2012

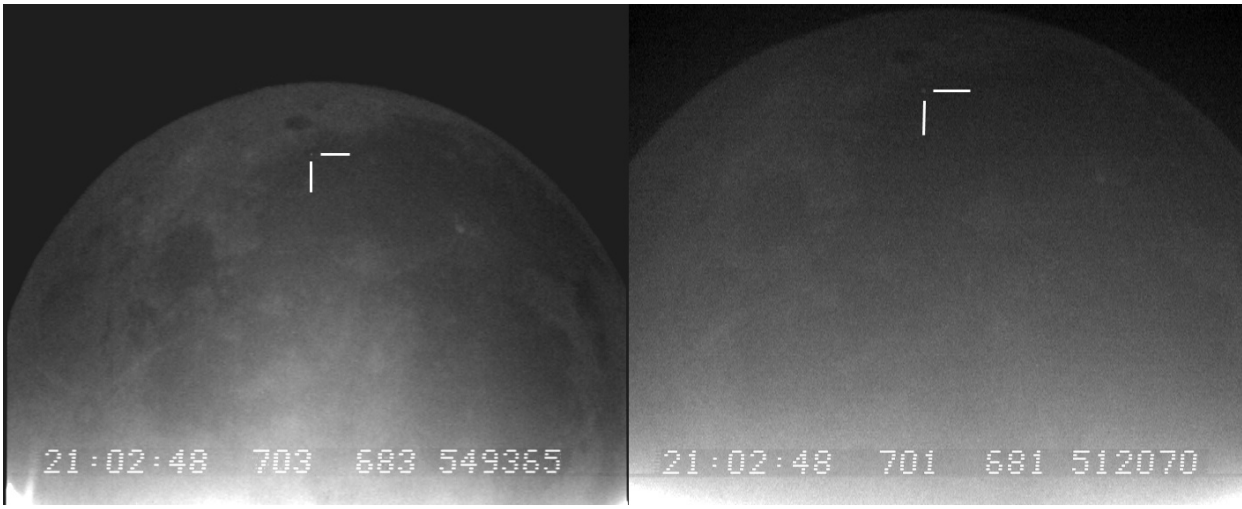

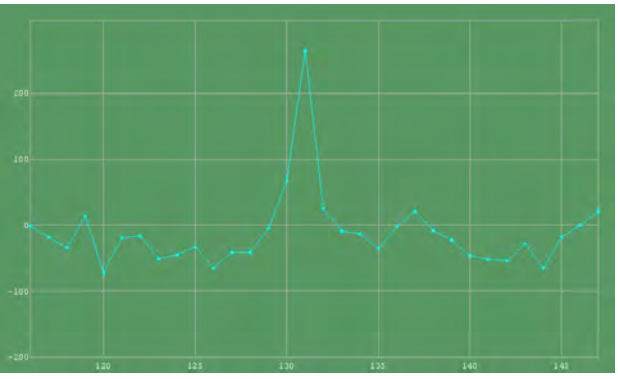

Image 3B. Lightcurve of the event N.3 of the Mar 28 2012

Selenology Today

Image 4A. Event N.4 of the Nov 20 2012

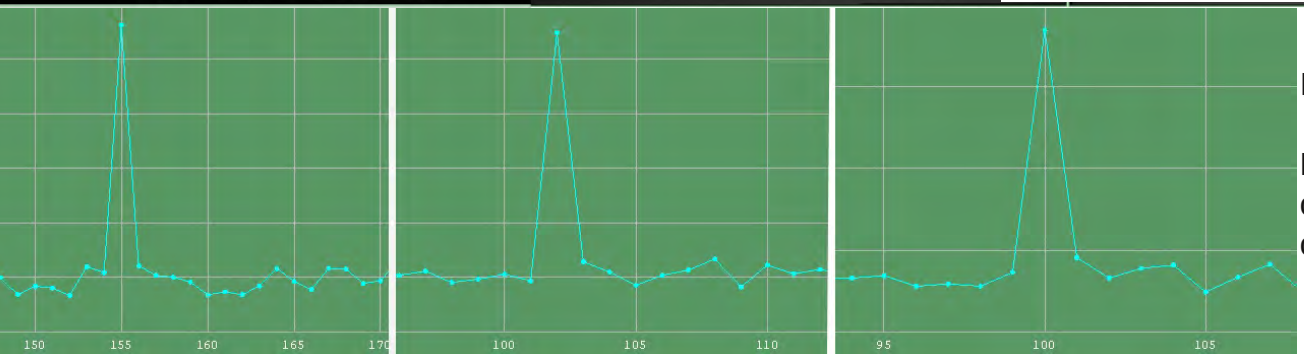

Image 4B.

Lightcurves of the event N.4 of the Nov 20 2012

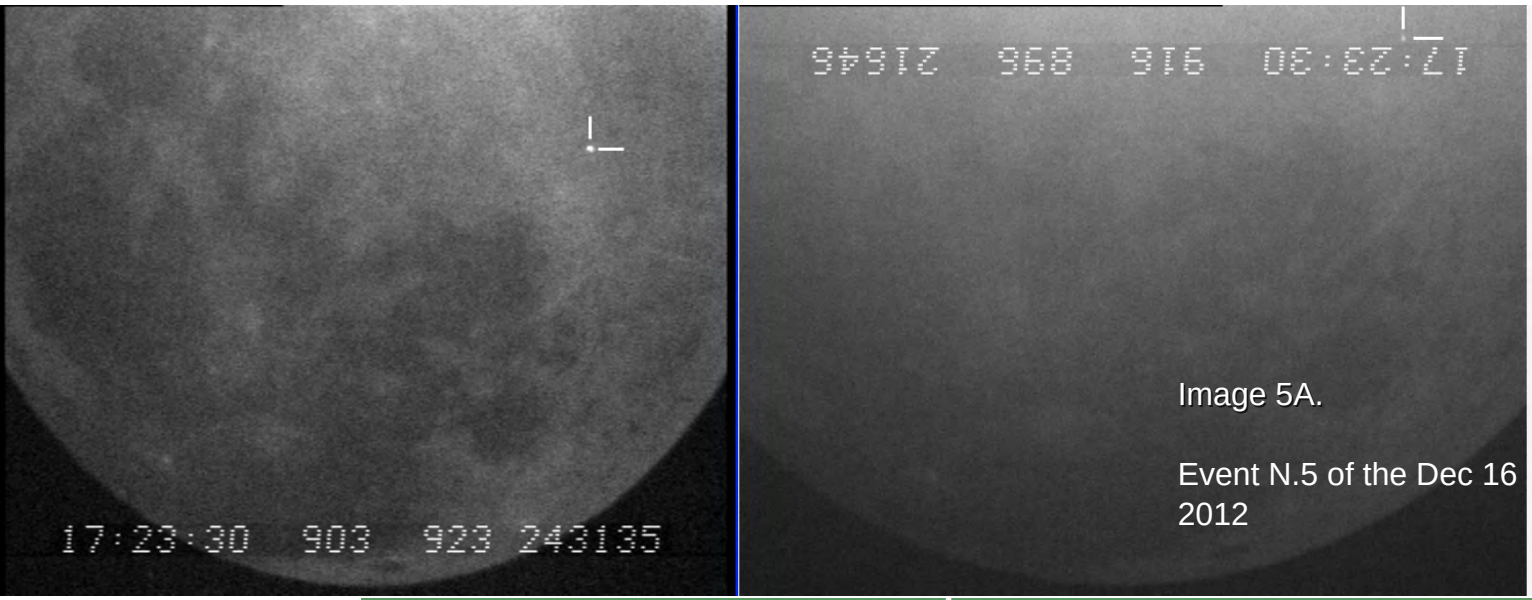

Image 5A.

Event N.5 of the Dec 16 2012

Image 5B.

Lightcurves of the event N.5 of the Dec 16 2012

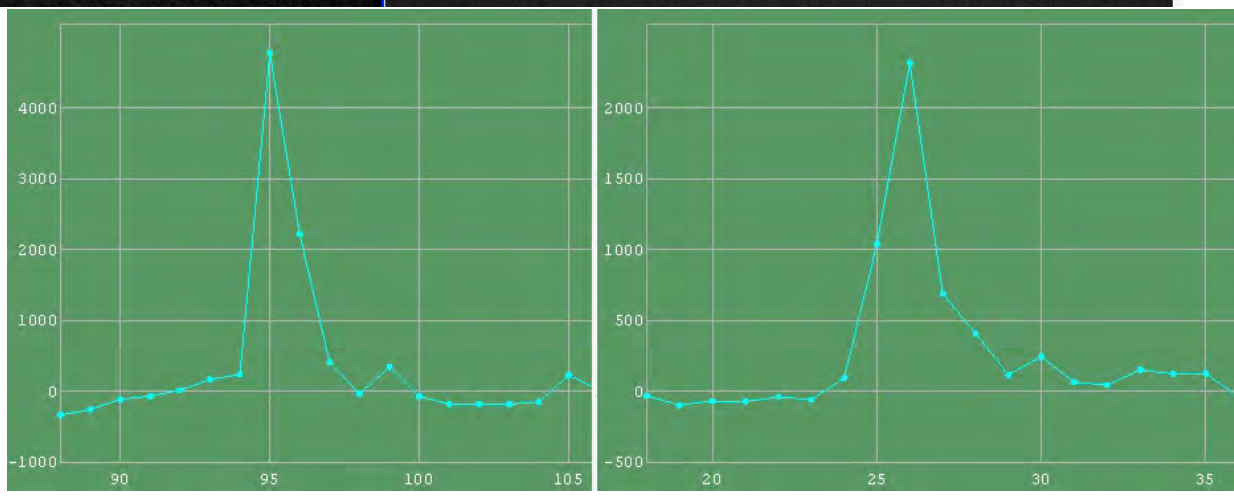

Selenology Today

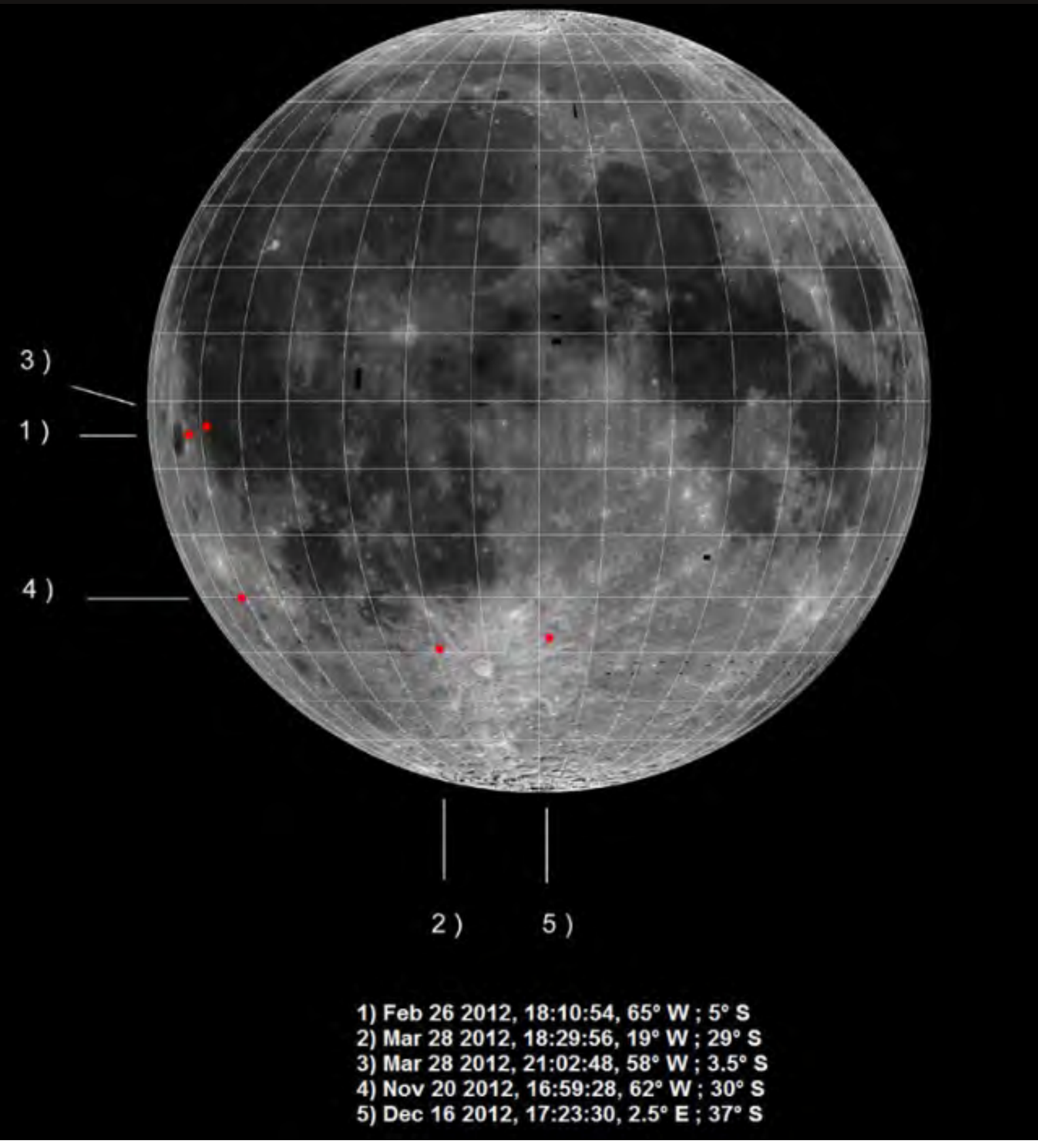

Image 6. Selenographic Coordinates of the events

	Event N. 1	Event N. 2	Event N. 3	Event N. 4	Event N. 5
Date	Feb 26 2012	Mar 28 2012	Mar 28 2012	Nov 20 2012	Dec 16 2012
UTC Time (hh:mm:ss)	18:10:54	18:29:56	21:02:48	16:59:28	17:23:30
Duration (s)	0,02	0,06	0,04	0,02	0,06
N. Fields	2	3	2	1	3
Magnitude (V)	not measured	9.3 +- 1.0	9.6 +- 1.0	not measured	saturated, under 7.0
Selenographic Coordinates	65° W ; 5° S	19° W ; 29° S	58° W ; 3.5° S	62° W ; 30° S	2.5° E ; 37° S
Remarks	Sporadic	Sporadic	Sporadic	Leonid? a Monocerotid?	Geminid? Comae Berenicid?
Captured in	2 telescopes	3 telescopes	2 telescopes	3 telescopes	2 telescopes
Moon Coordinates (Eq. 2000.0)	RA:01 51.6 DE:+14 25.9	RA:04 55.7 DE:+21 25.4	RA:05 00.2 DE:+21 19.0	RA:22 00.6 DE:-07 19.5	RA:20 48.4 DE:-13 14.5
Moon Horizon Coordinates	Az: 249 17 Alt: +37 51	Az: 245 17 Alt: +49 51	Az: 275 44 Alt: +24 38	Az: 172 13 Alt: +36 12	Az: 225 00 Alt: +18 57
Phase (%)	20,9	30,7	31,7	51,1	15,8
Air Mass	1,63	1,31	2,40	1,69	3,07
Moon angular diameter (arcmin)	29,6	29,7	29,7	31,2	32,3
Moon light distance (min)	0,022268	0,022107	0,022213	0,021117	0,020431
Observing Site 1 (M. Iten)	Gordola	Gordola	Gordola	Gordola	Gordola
Telescope Site 1	125mm refractor	125mm refractor	125mm refractor	125mm refractor	125mm refractor
Videocamera Site 1 (CCIR mode)	Watec 902H2Ult	Watec 902H2Ult	Watec 902H2Ult	Watec 902H2Ult	Watec 902H2Ult
Observing Site 2 (S. Sposetti)	Bellinzona (S. Corbaro)	Gnosca	Gnosca	Gnosca	Bellinzona (Liceo)
Telescope Site 2	200mm reflector	280 and 420mm reflector	280mm reflector	280 and 420mm reflector	280mm reflector
Videocamera Site 2 (CCIR mode)	Watec 902H2Ult	902H2Ult; 902H2Sup	Watec 902H2Ult	902H2Ult; 902H2Sup	Watec 902H2Ult
Moon parallax betw Site 1 and 2 (arcsec)	4,25	5,15	4,32	6,80	3,85
True distance betw Site 1 and 2 (km)	12,5	12,9	12,9	12,9	11,0
Apparent dist betw Site 1 and 2 (km)	8,3	9,9	8,4	12,5	6,9

Table 1.

Informations about the events, the Moon and the observing sites

References

Bellot Rubio, L.R., Ortiz, J.L., Sada, P.V., 2000. Observation and interpretation of meteoroid impact flashes on the Moon. EarthMoon Planets 82–83, 575–598.

Lena, R., Iten, M., Sposetti, S., 2011. Detection of three meteoroidal impact on the Moon. Selenology Today 24, 12-29.

Lena, R., Iten, M., Sposetti, S., 2011. Detection of two probable meteoroidal impacts on the Moon. Selenology Today 25, 60-65.

Melosh, H.J., 1989. Impact Cratering: A Geologic Process. Oxford Univ. Press, New York.

Melosh, H.J., and Beyer, R. A. 1999. Computing Crater Size from Projectile Diameter. http://www.lpl.arizona.edu/tekton/crater.html

Ortiz, J.L., Aceituno, F.J., Quesada, J.A., Aceituno, J., Fernández, M., Santos-Sanz, P., Trigo-Rodríguez, J.M., Llorca, J., Martín-Torres, F.J.,Montañés-Rodríguez, P., Pallé, E., 2006. Detection of sporadic impact flashes on the moon: Implications for the luminous efficiency of hypervelocity impacts and derived terrestrial impact rates. Icarus 184. 319-326.

Ortiz, J.L., Quesada, J.A., Aceituno, J., Aceituno, F.J., Bellot Rubio, L.R. 2002. Observation and interpretation of Leonid impact flashes on the Moon in 2001. Astrophys. J. 576. 567–573.

Sposetti, S., Iten, M., Lena, R. 2011. Detection of a meteoroidal impact on the Moon. Selenology Today 23, 1-32.

Steel, D., 1996. Meteoroid orbits. Space Sci. Rev. 78, 507–553.

Selenology Today

LUNAR DOME NEAR HUXLEY IN THE APENNINE REGION

Raffaello Lena, K.C. Pau Geologic Lunar Research (GLR) group.

Abstract

This study examines a lunar dome located near the crater Huxley. Based on a combined photoclinometry and shape from shading technique applied to telescopic CCD images acquired under oblique illumination, we determined for the dome a diameter of 14 km. The height amounts to 200 ± 20 m resulting in flank slopes of 1.64° ± 0.2°. Based on rheologic modelling we infer the physical conditions under which the dome formed (lava viscosity, effusion rate, magma rise speed) as well as the geometries of the feeder dikes. Huxley 3 formed from lava of viscosities of 1.8 x 10^6 over a period of time of 4.1 years. It is a C2 dome in the classification scheme of effusive lunar domes introduced by GLR group.

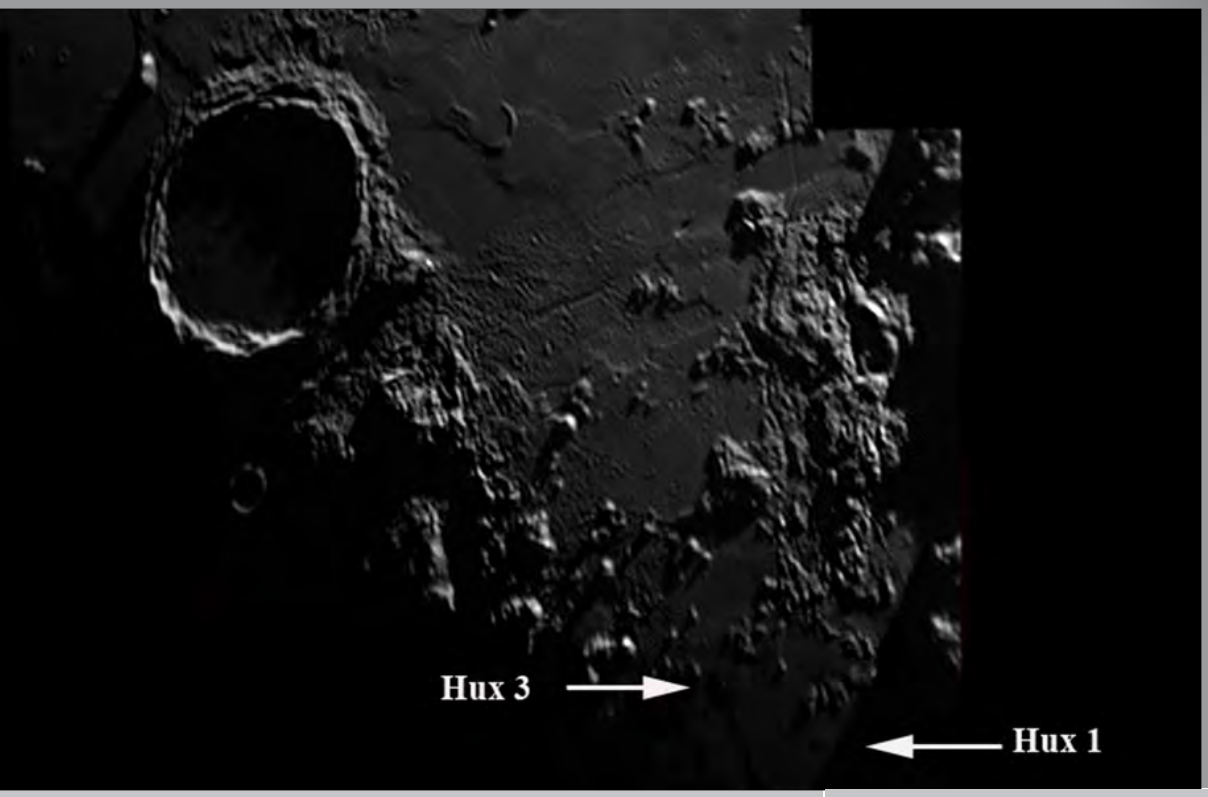

Figure 1.

The examined dome Hux3 with the nearby dome Hux1 (Lena)

Introduction

Effusive lunar domes formed during the terminal phase of a volcanic eruption. Initially, lunar lavas were very fluid due to their high temperature. Thus, they were able to form extended basaltic mare plains.

Lunar domes have been the subject of several preceding geologic studies discussed by GLR group (cf. Wöhler et al. 2006, 2007 and Lena et al. 2007, 2008).

In a previous study to appear in LPSC 44th conference (Wirths and Lena, 2013) an analysis of two low domes located in the Apennine region near the crater Huxley, termed Huxley 1 and 2, was provided. In this work we describe another dome, located nearby the preceding domes Huxley 1 and 2. Based on the telescopic CCD images we obtained a DEM of the examined dome by applying the combined photoclinometry and shape from shading method (sfs) and comparing the result with the LOLA DEM.

Telescopic CCD imagery

Fig. 1 displays a CCD images of the examined region including the dome termed Hux3.

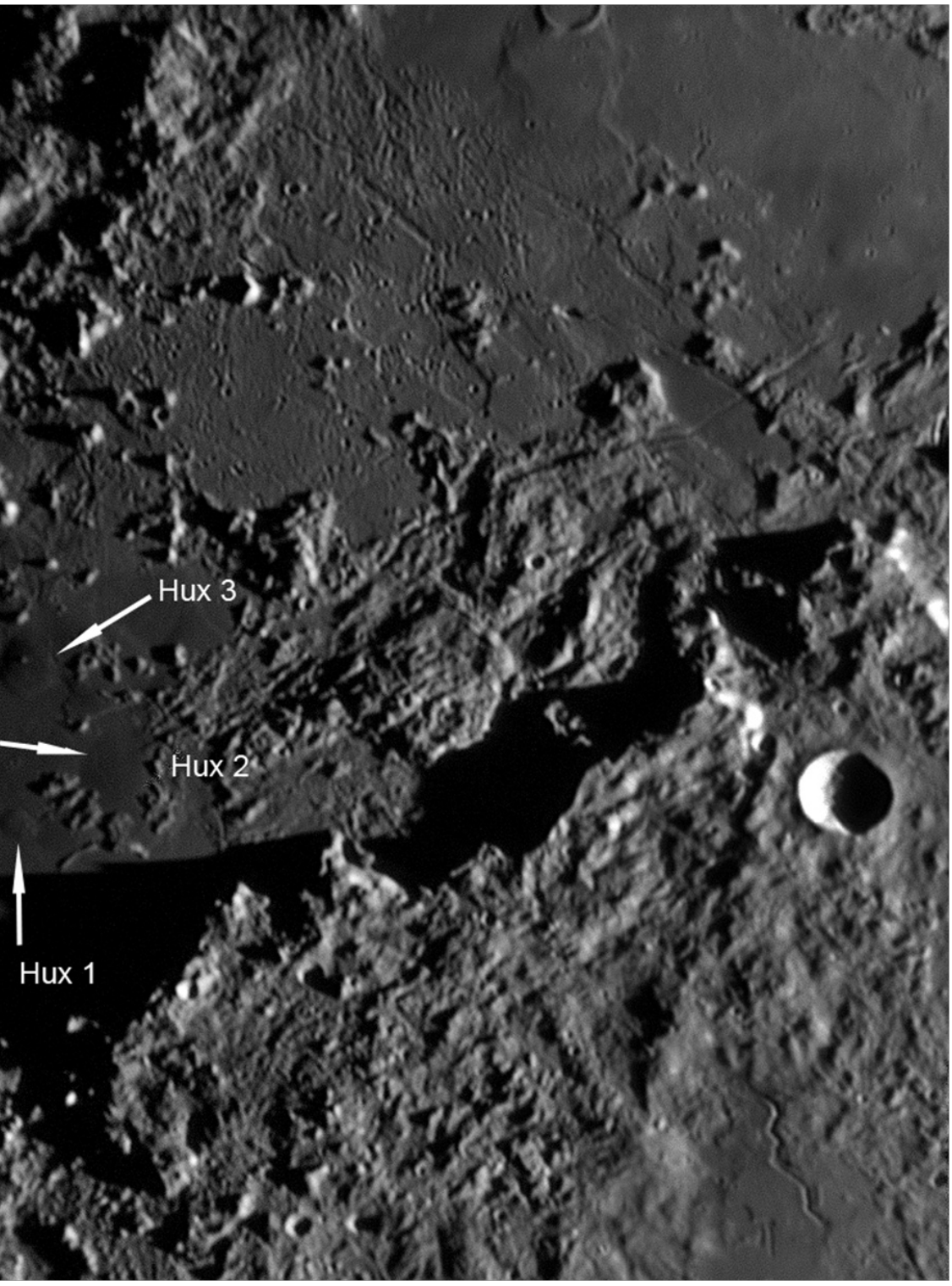

Figure 2.

The examined dome Hux3 with the nearby domes Hux1 and Hux 2 (Pau)

The images were taken with a 180 mm Mak-Cassegrain on November 11, 2012 at 17:23 UT (Fig.1) and with a 250 mm Newtonian reflector on December 21, 2012 at 11:35 UT (Fig.2). In the examined images also two domes Hux1 and Hux2 are detectable. All images shown in this article are oriented with north to the top and west to the left.

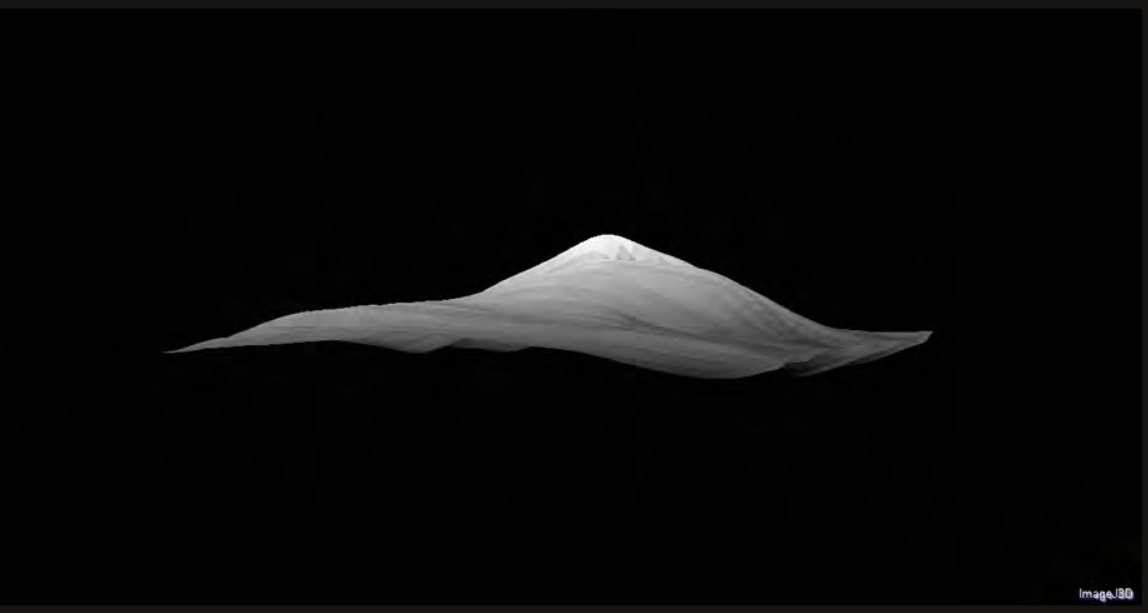

Figure 3.
3D reconstruction of the examined dome

Methods and analysis

- For spectral analysis, the Clementine UVVIS data were examined in terms of reflectance R_{750} at 750 nm and the R_{415}/R_{750} and R_{950}/R_{750} colour ratios. Albedo at 750 nm is an indicator of variations in soil composition, maturity, particle size, and viewing geometry. The R_{415}/R_{750} colour ratio essentially is a measure for the TiO_2 content of mature basaltic soils, where high R_{415}/R_{750} ratios correspond to high TiO_2 content and viceversa (Charette et al., 1974). The values derived for the examined dome are released on the calibrated and normalized Clementine UVVIS reflectance data as provided by Eliason et al. (1999).
The examined dome has R_{415}/R_{750} ratio of 0.5947 and R_{950}/R_{750} ratio of about 1.040.

- Lunar Orbiter images cannot be used for 3D reconstruction based on photometric methods such as photoclinometry due the nonlinear and unknown relation between incident flux and density of the film. Both Lunar Orbiter and Clementine images are characterised by illumination angles too steep to reveal very low topographic features. As a consequence, for an in-depth morphometric and subsequent rheologic analysis of the examined dome we performed a reconstruction of its 3D shape based on the available telescopic image data, using a combined photoclinometry and shape from shading method.

The photoclinometry approach takes into account the viewing direction of the camera, the illumination direction, and the surface reflectance in order to infer cross sectional profiles through the surface based on the observed pixel intensities (McEwen, 1991). These profiles are oriented along the azimuthal direction of illumination, corresponding to the image rows in the telescopic CCD images. Details about this approach and its application to the generation of digital elevation maps (DEMs) of lunar surface regions are given by Wöhler et al. (2006, 2007), Lena et al. (2007, 2008) and in the book by Lena et al. (2013). Furthermore, we estimated the magma rise speed U and the dike geometry (width W and horizontal length L) according to the modelling results routinely used for estimating the rheologic properties and dike geometries for a large number of monogenetic lunar mare domes by Wöhler et al. (2006, 2007) and Lena et al. (2007, 2008), where more detailed explanations about the model are reported.

Morphologic and morphometric properties

Morphology of the domes

The coordinates of the dome and its dimension was computed using the Lunar Terminator Visualization Tool (LTVT) software by Mosher and Bondo (2006). The LTVT software requires a calibration of the images by identifying the precise selenographic coordinates of some landmarks on the image. This calibration was performed based on the Unified Lunar Control Network (ULCN). The selenographic coordinates are determined to 21.26° N and 3.68° W.
The height of the dome Hux3 was determined to 200 ± 20 m, its diameter amounts to 14 km ± 0.510 km, resulting in flank slope of 1.64° ± 0.2° (Fig. 3). Assuming a parabolic shape the estimated edifice volumes correspond to about 22 km^3. Recently, a global lunar digital elevation map (DEM) obtained with the Lunar Orbiter Laser Altimeter (LOLA) instrument on the Lunar Reconnaissance Orbiter (LRO) spacecraft has been released
(http://pds-geosciences.wustl.edu/missions/lro/lola.htm).

A rendered image obtained using LTVT and the LOLA DEM, and assuming the same illumination conditions as in Fig. 1, is shown in Fig. 4. In the LOLA DEM, the elevation difference between the summit of Hux3 and the surrounding mare soil corresponds to about 190 m, which is in good agreement with our image-based photoclinometry and shape from shading. We also estimated the height of the dome based on shadow length measurements in the oblique illumination view shown in Fig. 1, where a value of 195 ± 20 m was computed.

Rheologic properties and classification

The model by Wilson and Head (2003) estimates the yield strength τ, i. e. the pressure or stress that must be exceeded for the lava to flow, the plastic viscosity η, yielding a measure for the fluidity of the erupted lava, the effusion rate E, i. e. the lava volume erupted per second, and the duration of the effusion process T. The computed

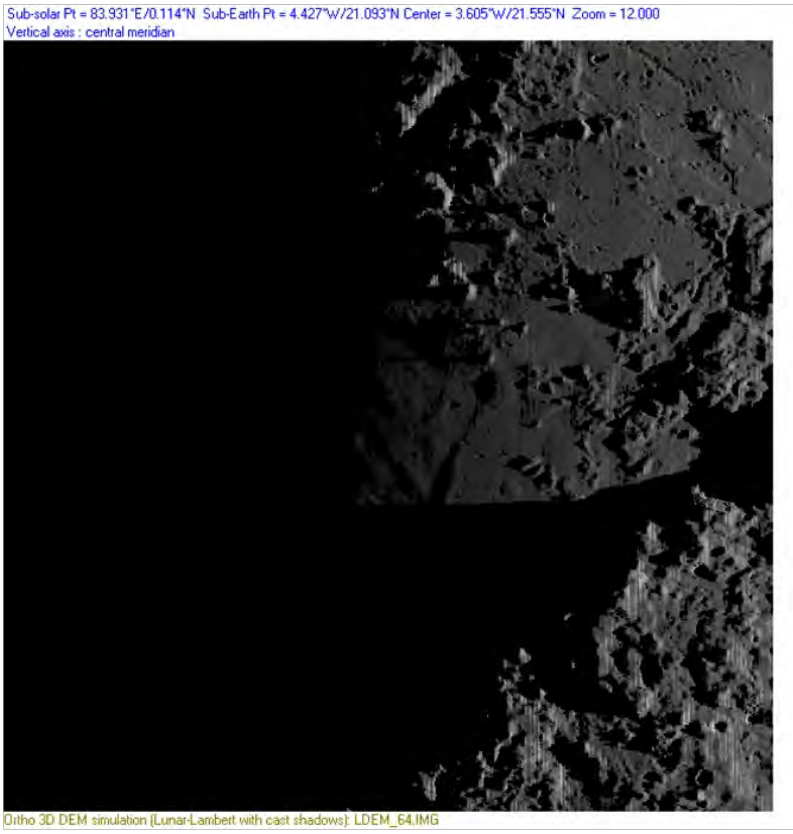

Figure 4.
A rendered image obtained using LTVT and the LOLA DEM, and assuming the same illumination conditions as in Fig. 1

values are valid for domes that formed from a single flow unit (monogenetic volcanoes). Based on the morphometric properties of the examined dome we obtain for Hux 3 lava viscosity of 1.8 $x10^6$ Pa s, a lava effusion rate of E = 170 m^3 s^{-1}, and a duration of the effusion process of T = 4.1 years. The magma rise speed amounts to U = 2.3 x 10^{-5} m s^{-1} and the dike width and length to 55 m and 180 km, respectively.
These rheologic values were inferred assuming the minimum vertical magma pressure gradient of dp/dz = 328 Pa m^{-1} required to drive magma to the lunar surface as reported by Wilson and Head (2003). The dome Hux3 belongs to the class C2 in the GLR classification scheme of lunar domes (cf. Lena et al., 2013).

References

Charette, M. P., McCord, T. B., Pieters, C., & Adams, J. B., 1974. Application of remote spectral reflectance measurements to lunar geology classification and determination of titanium content of lunar soils. Journal of Geophysical Research, 79 (11), 1605–1613.

Eliason, E., Isbell, C., Lee, E., Becker, T., Gaddis, L., McEwen, A., & Robinson, M., 1999. Mission to the Moon: the Clementine UVVIS global mosaic. PDS Volumes USA NASA PDS CL 4001 4078. http://pdsmaps.wr.usgs.gov

Lena, R., Wöhler, C., Phillips, J., Wirths, M., Bregante, M.T., 2007. Lunar domes in the Doppelmayer region: spectrophotometry, morphometry, rheology and eruption conditions. Planet. Space Sci. 55, 1201–1217.

Lena, R., Wöhler, C., Bregante, M.T., Lazzarotti, P., Lammel, S., 2008. Lunar domes in Mare Undarum: spectral and morphometric properties eruption, conditions, and mode of emplacement. Planet. Space Sci. 56, 553–569.

Lena, R., Wöhler, C., Phillips, J., Chiocchetta, M.T., 2013. Lunar domes properties and formation processes,Springer (toappear) http://www.springer.com/astronomy/astrophysics+and+astroparticles/book/978-88-470-2636-0

McEwen, A. S., 1991. Photometric Functions for Photoclinometry and Other Applications. Icarus, 92, 298–311.

Mosher, J., & Bondo, H., 2006. Lunar Terminator Visualization Tool (LTVT). http://inet.uni2.dk/d120588/henrik/jim ltvt.html

Wilson, L., and Head, J. W., 2003. Lunar Gruithuisen and Mairan domes: Rheology and mode of emplacement. Journal of Geophysical Research, 108 (E2), 5012, doi:10.1029/2002JE001909.

Wirths, M. and Lena, R. 2013. Lunar Domes in the Apennine Region near the crater Huxley: Morphometry and mode of formation. Lunar and Planetary Science Conference XXXXIV, abstract #1006

Wöhler, C., Lena, R., Lazzarotti, P., Phillips, J., Wirths, M., & Pujic, Z., 2006. A combined spectrophotometric and morphometric study of the lunar mare dome fields near Cauchy, Arago, Hortensius, and Milichius. Icarus, 183, 237–264.

Wöhler, C., Lena, R., & Phillips, J., 2007. Formation of lunar mare domes along crustal fractures: Rheologic conditions, dimensions of feeder dikes, and the role of magma evolution. Icarus, 189 (2), 279–307.

Selenology Today

Advanced lunar image processing techniques: Salvaging images taken under poor conditions.

By Maurice Collins

In this article I would like to share with you some of my techniques for processing lunar images that were acquired under less than ideal atmospheric conditions, namely through thin clouds.

Capturing images when cloud covers the Moon

Often here in Palmerston North the weather changes suddenly from clear sky to cloudy in a matter of minutes, especially just after sunset. Sometimes it is right in the middle of a lunar full disk mosaic that was started when the Moon was in the clear. Often it is still possible to complete the mosaic and continue imaging up until the Moon is too dim to see on screen (though it may still be visible to the eye) and show you how to correct these later on in post processing. The following will describe the way I proceed under these adverse conditions.

Cloud passing over the Moon is a sure way to ruin images and will cause parts of the image to be brighter than others in each frame as different densities of cloud pass through the field of view. Don't give up, unless you can see a big hole approaching in a few minutes. Continue to take frames as normal but increase the light level slider from 255 to say 150 or so depending on the dimness of the image. Also increase the exposure time to compensate if necessary. Be aware however that if a clearer patch appears, it will overexpose what would have been a very good frame, so use that only if consistently clouded out. Hopefully the image will not get too grainy, but it will be noticeable all the same, but this will be compensated to some degree later during stacking which reduces noise. If you get some good frames captured with little cloud these may be enough even if only a few frames, for that section of the Moon. Cloud around the Moon will increase the brightness of the surrounding space as the moonlight reflects off it, giving low contrast. This can also be fixed later. If the cloud is thin it will only act as a light attenuation filter and the images will come out almost normal. It is the dark black clouds cutting of the lunar light totally that make it more difficult. When the Moon is totally obscured it is time to stop and wait a while to see if it clears. However, as long as craters are still visible, in most cases the images can be salvaged in post processing. So keep imaging until all hope is lost and the Moon is gone behind the clouds!

Stacking the images

For less than perfectly clear images I have found it necessary to use Registax 5. The latest version is ver 6 and it uses a different technique for stacking images, taking sections of each image and combining the best parts. With parts of the image obscured by clouds this makes for a polygon shaped jigsaw puzzle looking final frame, which is not useable. So only the older version of Registax stacks all of the frames on top of each other, averaging the results, so this is the one we need to use in this instance.

Stack the images as you normally would, the limit function at default settings will like to discard more images than necessary in most cases.

So if it automatically says to stack only 2 or so images, bypass this and move the slider to the right until it includes as many images of acceptable quality (ie you can still see the Moon reasonably brightly). Then accept that limit and Optimize and Stack. It will then average the bright and dark frames. So try to keep more brighter frames and less darker. The final frame then will need some further adjustments in Registax. Got to the Gamma function button and on the graph increase the brightness of the image by bending the curve upwards in the middle. Apply it to all the frames using the “Do All” button. (It will remember this setting for subsequent frames, but since they may be different, just press reset on them before you apply the curve). Then adjust the wavelets sharpening on the image to suit the quality of the seeing. Apply the “Do All” button once again and save the frame. It could be possible to do even more of the processing in Registax if you wish, but at this point I pass it onto Photoshop to do the rest. Do this process for all of the frames for the mosaic (which hopefully will be complete – I check by picking one frame of each image and stitch as a test before going to work on this just to be sure). Launch Photoshop software or you favourite image processing software (GIMP, Maxim DL, etc). The techniques that follow should be common to all as very basic in approach.

Post-Processing

Now you have all your images stacked and in reasonable quality, both those taken before the clouds came and those afterward, it is time to fine tune them to make them look roughly the same so they can be mosaiced into a full image of the Moon.

Open one of the good images and one of the cloud affected images together in Photoshop. Now using the “Curves” function (Ctrl-M) to adjust the brightness levels bring the brightness of the clouded image to match that of the non-affected image. If this is an area of the lunar limb it will bring up the brightness of the cloud scattered light surrounding the Moon, making the black of space light grey or yellowish. That is ok, we can fix that up later. Open up the levels (Ctrl-L) tool and click on the left hand most eyedropper to select a black cutoff point. Then click on the black of space surrounding the Moon. This will set it to black as it would be without clouds, but it may also alter the colour of the Moon. If so, click again on a different point as it is picking up one of the RGB pixels and altering the lunar colour unevenly. Just pick some point that has the least affect. If none work, cancel, and start again with levels, but this time just move the black cut-off slider to the right to dim down the black to a reasonable level of darkness. Save the image. Also if the frames have stacked and made the edges like a series of nested frames of differing brightness, which happens if there is drift in the mounting which is common with my ETX-90 as the tracking is not very smooth. Crop the frame to get the best portion of it, to avoid problems later with stitching. It may also be necessary to increase the brightness with curves again to increase the contrast of the image as setting the sky to black may have lost too much detail in the image and dimmed the image too much.

Now work your way through each frame, trying to make it as good as the reference frame as possible. This does not have to be exact. Just get it within a ball-park of the good frame and the stitching software should take care of the final adjustments later.

Frames taken near the centre of the Moon without a limb region are the more difficult as there is no region to set a black point and so I do it with Curves, even setting cutting off the black values by moving the base of the curve to

clip the data. Or use a combination of levels and curves to get it looking right. Sharpening will also help improve the contrast, and you can also use the “Brightness/Contrast” slider controls and in some cases the “Shadows and Highlights” function will helps bring up the brightness, at the expense of noise. It is possible to do some noise reduction also, but I rarely do until the final stitched mosaic is together.

Making the mosaic

Now that you have all the frames looked reasonable with lunar detail visible in all frames, it is time to see if the mosaic will work. Assuming you got the whole of the Moon, I use Microsoft Image Composition Editor (ICE) to make my mosaics. Stitch all the frames that are good (and if you have some of the same region varying in quality, select and de-select to get the best ones to stitch). The mosaic preview will appear, check it looks all there and correct. Sometimes under low contrast it can fail miserably and substitute craters where they are not in reality! Now, try exporting at 100% size. This may or may not work. If the final stitch mosaic shows up the joins of varying brightness and contrast, then 100% will not be possible for this mosaic. But that is usually ok, a 75% size will be a good image to start with all the same. So select that size to export and examine it again. This image should then be uniform in brightness if the ICE software has done its job with your fixed frames. Take this mosaic into Photoshop or your favourite image processing software and adjust the brightness of the whole image with curves again, apply some “smart sharpen”, I usually use 20% at about 1.5 pixels but it depends. Apply it again at lower settings, 12%, 0.8px for fine detail improvements. Also select any really bad regions separately and apply it only to that region, same for noise reduction. Set the black point of the general black space and then clean up the surrounding space using the select area tool with a feather (fading the edges so not a sharp edge) and pressing “delete” with the background colour set to pure black. This removes any remaining faint edges to the stitched frames that always show up on all stitched mosaic frames with my imager, yours may be less noisy. Then set the black point of the space. If this darkens the image too much, try using the circular tool to select the whole of the Moon just out from the limb with a feather setting of 10 px and then “inverse selection” so you are now selecting the black of space and press “delete”. This removes most of the extraneous light outboard of the lunar limb and just leaves a bright area next to the limb, which can be left there or reduced in brightness with levels to a lesser extent. Sometimes it is necessary to bring out the terminator with the “Shadows and Highlights” tool but apply it sparingly as it also increases noise, which will be quite high anyway due to the clouds. Also it may be necessary to correct for the colour of the image (for colour imagers) as it may be too yellow, brown or blue (if taken in twilight). Usually clouds make it more yellow/brown than it should be. Sometimes this effect is ok, as that is what it looked like visually with a bit of cloud, so only fix it if it bothers you. In bad cases discard the colour entirely and make it a black and white image (if you have a mono imager this will of course not be an issue). Usually this increases the noise considerably with a one shot colour camera such as the Meade Lunar and Planetary Imager (LPI) that I use, and it may be necessary to apply some noise reduction. Also as the 75% size image may still show up flaws it may be advisable to reduce the size of the image further to sharpen it up, just as you would use a lower magnification eyepiece under poor atmospheric seeing condition to get the sharpest image. Try a reduction of 75% or 67%. It is usually quite an improvement to the overall look of the image.

Selenology Today

Finishing up

Now all that remains is to put the details of the image, the date, time in UT (start and end time the frames covered), telescope aperture, imager, observers name and location, crop the black space evenly around the Moon, and you are done! Now you have a usable image to share on your favourite email newsgroup, and the BAA and ALPO lunar sections are also keen to get any images you have. Details are on their websites.

Hope some of these techniques help you salvage some observing sessions that at first appeared to be ruined by the whims of nature. With the magic of image processing you can persevere may have a nice image to share at the end of it that few would believe was taken with clouds in the way!

14.5-day Full Moon
2011 June 16
0901 - 1017UT
Thick haze
C8 & LPI
Maurice Collins
Palmerston North, NZ

Selenology Today

Archytas G Concentric Crater

by Howard Eskildsen

Abstract

Archytas G concentric crater in Mare Frigoris has a diameter (D) of 7.0 km, a depth (d) of 0.44 km and a depth to diameter (d/D) ratio of 0.062. The north rim of a slightly smaller crater intersects the south rim of Archytas G. The smaller crater has a diameter of 4.3 km, a depth of 0.30 km and a depth to diameter ratio of 0.070. The toroid (T) or inner ring of Archytas G is 4.5 km for a T/D ratio of 0.63 and the smaller crater to the south has a toroid diameter of 2.2 km for a T/D ratio 0.51. The two craters appear to be of similar age and have had similar distortion of their original depths and may possibly be double impact craters.

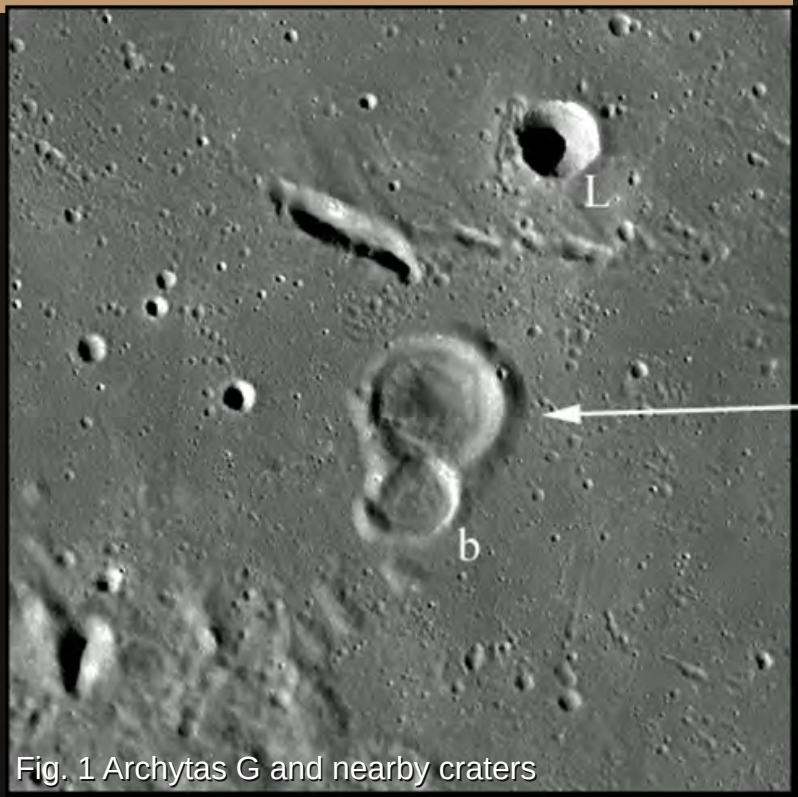

LROC WMS Map

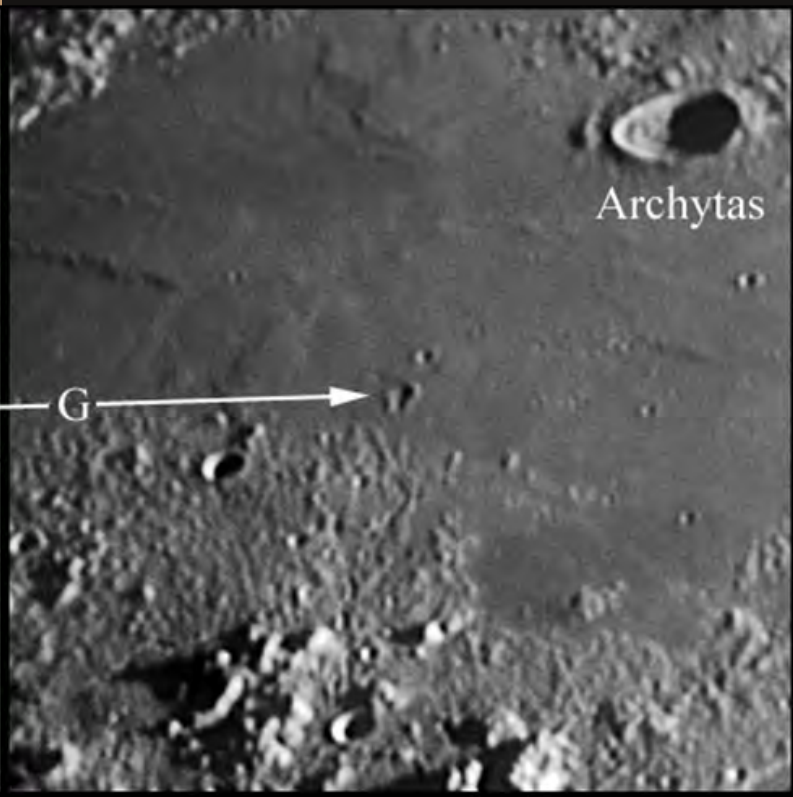

2010/09/17, 00:44 UT, Seeing 5/10, Transparency 4/6,
6" f/8 Refractor, Exlpore Scientific Lens, 2X Barlow, Losmandy GM8 Mount
JMI Electric Focuser, DMK 41AU02.AS, W-8 Yellow Filter
Howard Eskildsen, Ocala, Florida, USA

Fig. 1 Archytas G and nearby craters

Methods

Depths and diameters of the crater and their inner ring toroids (Table 1) are from LROC Act-React QuickMap surface profiles (Fig. 2). Lowest central crater elevation was subtracted from the mean of four rim elevations (Table 2) to determine depth in kilometers.

Diameter is the mean of the geodetic distances from the north to south rims and the east to west rims of the craters and the inner toroid rims as determined using the LROC Act-React QuickMap (Table 3). The d/D ratio accuracy is limited to two significant figures. Coordinates from the QuickMap (Table 1) compared with the LROC WMS Image Map agreed to within 0.02°. Geodetic distances were used since cartographic distances were distorted by the map's cylindrical projection.

Precision of the data is limited by the variations of the diameter of the crater rim depending on the direction of measurement, the indistinct rims of the inner toroids, and the variability of the surface profiles depending on the exact location of the lines of measurement.

Data

		LROC	Crater			Toroid (T)	
	Wood	QuickMap	Depth (km)	Diameter	d/D		
Crater	Coordinates	Coordinates	(d)	(D)	Ratio	Diameter	T/D Ratio
Archytas G	0.4E 55.8N	0.53E 55.74N	0.435	7.0	0.062	4.5	0.63
Archytas G-b	Not on List	0.48E 55.56N	0.304	4.3	0.070	2.2	0.51
Archytas L	Not concentric	0.91E 56.19N	0.633	4.0	0.159		

Table 1: Crater Coordinates and Dimensions

					Mean Rim	Central
	Geodetic Crater Rim Elevation				Elevation	Elevation
Crater	North (m)	South (m)	West (m)	East (m)	(meters)	(meters)
Archytas G	-2680	-2490	-2690	-2440	-2575	-3010
Archytas G-b	-2650	-2680	-2066	-2550	-2486.5	-2790
Archytas L	-2640	-2680	-2680	-2630	-2657.5	-3290

Table 2: Crater Rim and Central Floor Elevation Measurements

	Geodetic		Geodetic	
	Crater Diameter		Toroid Dameter	
Crater	N-S km	W-E km	N-S km	W-E km
Archytas G	6.98	7.05	4.33	4.57
Archytas G-b	4.12	4.56	2.11	2.30
Archytas L	3.87	4.11		

Table 3:
Crater and Toroid (Inner Rim) Measurements

Fig. 2 Surface profiles of Archytas G, Archytas G-b and Archytas L from LROC Act-React QuickMap

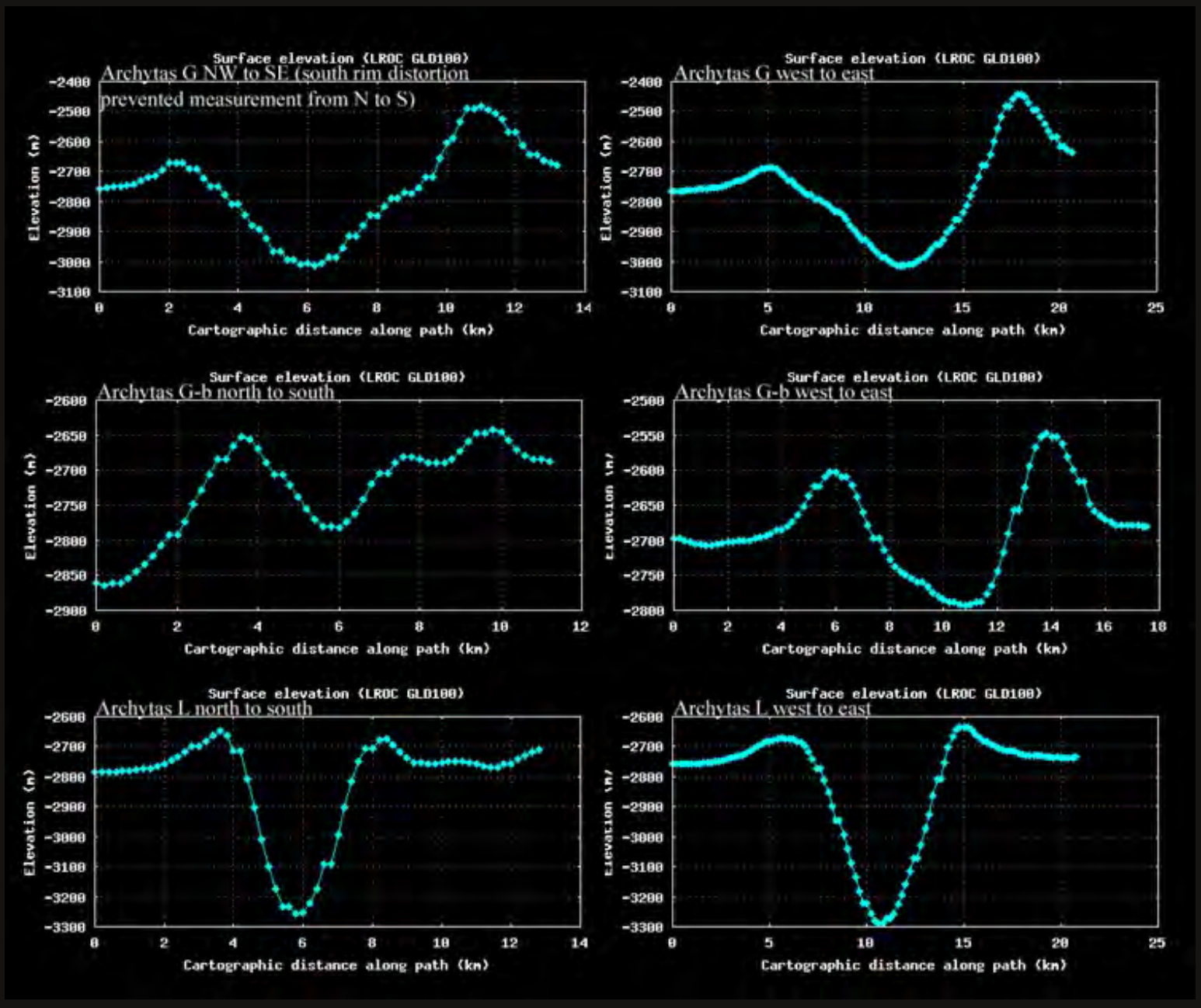

Comparison Data for Archytas G:

Source:	Coordinates:	Crater Rim Diameter (D):	T/D Ratio
Study Data Above	0.53E 55.74N	7.0 km	0.63
Wood, C. (1978)	0.4E 55.8N	6.8 km	0.54
Losak, A. (2009)	0.5E 55.6N	7.0 km	Not available
Wöhler and Lena (2009)		6.8 km	0.59 (calculated from their data)

Selenology Today

Discussion

Archytas G is pictured in Fig. 1 with the LROC image left and 6" refractor image on the right. It is the first concentric crater on Chuck Wood's list published in 1978. It lies atop a lunar dome (Lena et al., 2008, Wöhler and Lena, 2009) which is just barely visible in refractor image. It is located at the southern margin of Mare Frigoris northeast of Plato at 0.53E, 55.74N, and its concentric appearance is visible on the orbiter image, but not on the refractor image. It is possible that its concentric appearance might be visible from larger telescopes under ideal conditions. It has a depth of 0.44 km, mean diameter 7.0 km with a depth/diameter ratio (d/D) of 0.062. A smaller crater merges with its southern rim and has been labeled Archytas G-b for discussion purposes. Its depth is 0.30 km, mean diameter 4.3 km, and d/D 0.070.

Both craters are on the lunar dome, are quite worn and appear to be very ancient, have had similar disruption of their crater floors, and have similar depth/diameter (d/D) ratios that are smaller than would be expected for craters their size. Spectral studies show that their floors have a spectral signature more like the adjacent highlands than the surrounding mare basalt (Lena et al., 2008). Their similarities suggest that whatever made G a concentric crater also altered the floor of G-b in a similar manner.

The similarities of Archytas G and G-b raise the question if they were a double impact. Perhaps G-b should be considered a concentric crater as well; if so, they would be the only pair of concentric craters that I am currently aware of. The age of the pair would be less than the age of the mare deposits they are in, but considerably older than Archytas L, so would be constrained between 3.8 billion and 1 billion years, but probably much older than the lower date. Conceivably three million millennia or more may have passed since the pair first appeared on the Moon.

For comparison, the slightly smaller crater, Archytas L (depth 0.63 km, mean diameter 4.0 km, d/D 0.16), just to the north has a more normal appearing floor with a d/D ratio more than double that of Archytas G and G-b. It is much less worn and considerably younger than the other two, but its absence of rays suggest that it is at least a billion years old. Perhaps the conditions that altered the floors of G and G-b ceased to exist before L was formed. This would be consistent with both the igneous intrusion and the igneous extrusion hypotheses of concentric crater formation.

References

1. Lena, R., Phillips, J., Bregante, M.T., Lammel, S., and Tarsoudis, G., 2008. A study about two domes near craters C. Herschel and Archytas, and an effusive dome in Mare Frigoris. Selenology Today 11, pp. 4-14.

2. Losiak, A., Lunar Impact Crater Database v9Feb2009.

2. Wöhler, C and Lena, R., 2009. The Lunar Concentric Crater Archytas G Associated with an Intrusive Dome. Lunar and Planetary Science Conference XXXX. Abstract1091, The Woodlands, Texas.

3. Wood, C.A., 1978. Lunar Concentric Craters. Lunar and Planetary Science Conference IX

Selenology Today

Adams B - A possible hybrid crater.

Barry Fitz-Gerald
GLR Group

Abstract

Crater formation in the Solar System is subject to a number of factors relating to both the projectile and the target. Among the factors relating to the projectile, impact angle is significant, with a large population of oblique impact craters identified on the terrestrial planets (Bottke et.al, 2000). In addition, there is an increasing appreciation that not all impactors are single bodies, and that binary (and possibly even more complex multiple configurations) asteroids exist and can result in simultaneous multiple impact craters which also exhibit their own characteristic features (Bottke, and Melosh,1996 and Oberbeck 1973). This article proposes that Adams B represents a possible example of an oblique multiple impact and cites its unique planform and ejecta to support the proposal.

Adams B, is an elongate crater measuring some 36kms long by 27kms wide located on heavily cratered highland terrain some 150kms to the south-west of Petavius. The surrounding terrain is dominated by ejecta, secondary craters and crater chains possibly formed by the Petavius impact event. Adams B itself appears to be one of the youngest features in the region, with a fresh sharp rim, and conspicuous impact melt floor. There are numerous bright rays crossing the area including a large conspicuous bright ray that appears to be associated with the northern rim of Adams B, and has been proposed as possible evidence of an oblique impact origin for the crater (Wood, 2012).

Oblique impacts are known to result in elongate crater-forms, and an asymmetric distribution of ejecta including the production of the lateral 'butterfly wings' of the type seen in the crater Messier and discussed by Gault and Wedekind (1978). Simultaneous multiple impacts were investigated by Oberbeck (1937) whilst Oberbeck and Morrison (1973 & 1974) continued the study of multiple impacts with particular reference to the formation of secondary craters. They identified diagnostic features visible in both primary and secondary simultaneous impacts. Amongst these features are 'V' shaped ridges resulting from the interference of the ejecta from the overlapping transient cavities.

These ridges result in the 'herringbone' pattern typical of secondary impact craters, and are visible in primary craters as extended filamentous rays that can extend for some considerable distance from the parent craters.

As can be seen from the LRO Quickmap image of Adams B shown in Fig.1, the crater outline is not a simple ellipse as might be expected from a low angle impact of the Messier type, but appears to be composed of three overlapping craters arranged in a line, a larger central one with smaller ones to the north-west and south-east. For ease of labeling I shall refer to the north-western crater as A, the central one as B and the south-eastern one as C. The individual nature of each crater is suggested by 'pinches' in the crater rim where the radius of curvature of each crater differs. Two of these points marked P1 and P2 appear to mark the contact between craters A and B whilst P3 appears to mark the junction between B and C. The fact that the junction between B and C's southern rims is not marked by a 'pinch' in the rim which would correspond to P4 may be a result of rim erosion by wall slumping into the crater interior. I will however label this area P4(?) for ease of future reference.

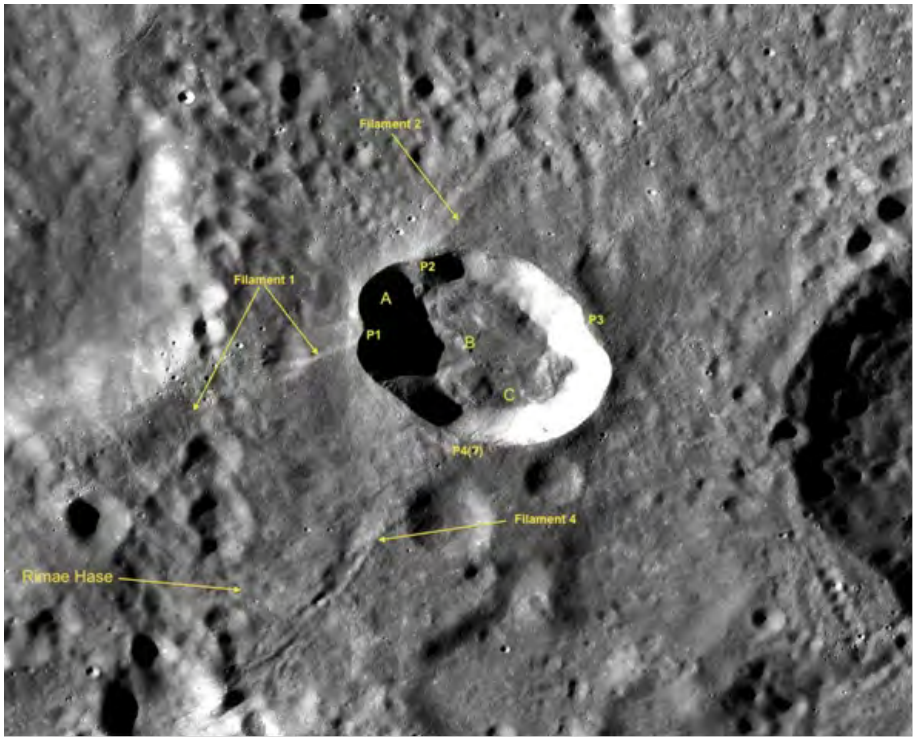

Fig.1 LRO Quickmap image of Adams B showing division into three sub-units A, B and C, the three filamentous rays (Filament1,2 &4), and 'pinched' sections of rim P1,P2 and P3. It is proposed that a similar pinched section at P4(?) is missing due to wall slumping. The crater to the right of the frame is Adams.

Adams B's ejecta can be seen to contain a number of long filamentous rays which appear to originate from positions on the rim previously identified as being the junctions between craters A, B and C. As can be seen from Fig.1, Filament 1's origin corresponds to P1, Filament 2 (which is subdued) to P2 and Filament 4 to P4(?). These filaments appear to be composed of ridges of irregular height which display complex branching structures (Fig.2A) or in places a feint hint of a herringbone patterning (Fig.2B). The correspondence between these filaments and the proposed junctions between the separate crater units strongly suggests that Adams B was created in a simultaneous triple impact, with Filaments 1 and 2 being produced by the interaction of the expanding ejecta blankets of A and B and Filament 4 being produced by the interaction of those of B and C.

A more detailed examination of the area to the north of Adams B shown in Fig.3 reveals an extensive ejecta deposit extending from the craters northern rim. This ejecta smothers pre-existing Petavius secondary craters and itself contains numerous secondary chains derived from Adams B in addition to the rather obscure Filament 2.

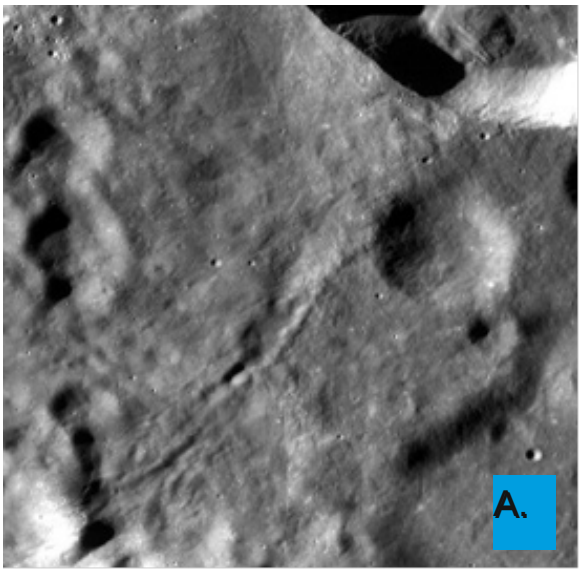

Fig.2.
A - Detail of Filament 4 showing irregular height and branching structure distally
B - Detail of Filament 1 showing feint 'herringbone' type patterning

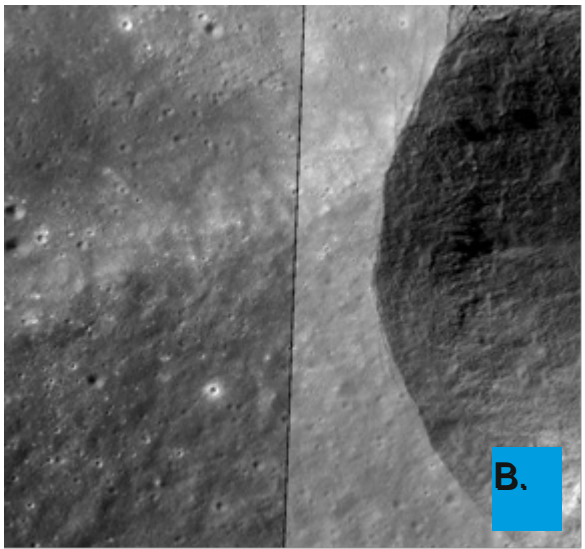

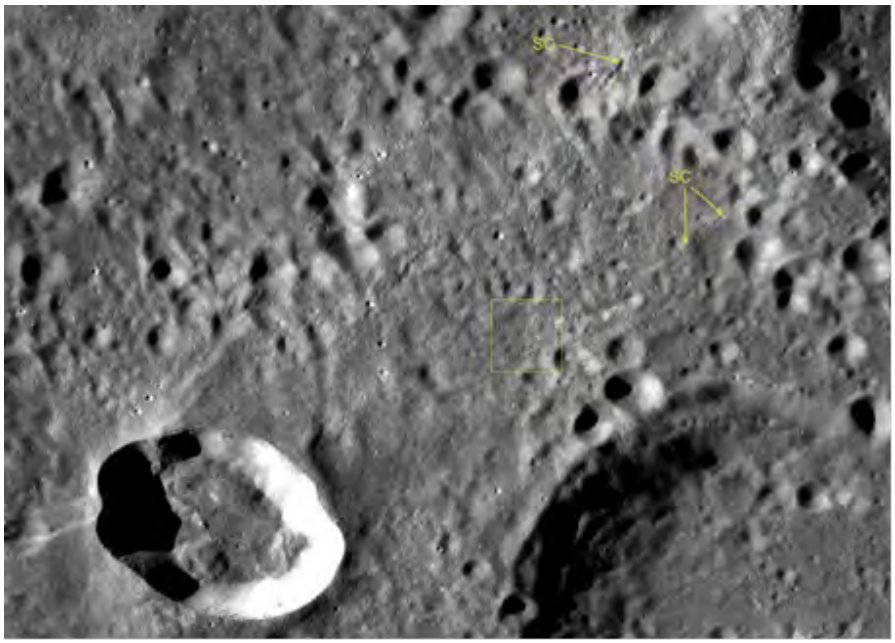

Fig.3 Ejecta to the north of Adams B. Showing secondary craters (SC) some 80kms distant from the crater rim.

Some of these crater chains, appear to extend from the rim for over 80kms, (Fig.3 feature SC) and may represent sections of filament type rays, of which Filament 2 may be a proximal section. Close to the rim these crater chains and the intervening ridges appear to be obscured by later ejecta deposits. That this may be the case is shown by the observation that hummocky deposits overly the crater chain/ridge striated ejecta proximally as shown in Fig.4 .This may be interpreted as an initial sequence of ejecta, which produced a striated terrain composed of crater chains and ridges, possibly formed by ballistic erosion during the early phases of crater excavation. This was followed by the deposition of a proximal hummocky ejecta that smothered these earlier deposits at a later stage of the crater forming process. The result is that the striated terrain is buried beneath this hummocky ejecta proximally, and only becomes obvious distally when the hummocky ejecta thins out. The lack of well developed filaments to the north may therefore be a consequence of a greater depth of obscuring hummocky proximal ejecta. To the south a comparatively reduced proximal blanket resulted in Filaments 1 and 4 being more visible.

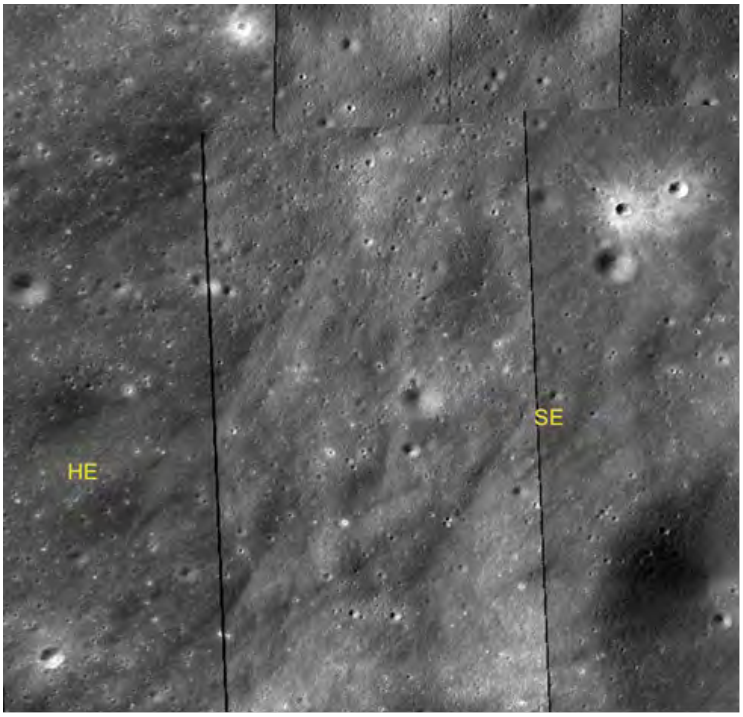

Fig.4
Detail of box in Fig.3 showing proximal hummocky ejecta (HE) overlying striated crater chain/ridge deposits (SE).

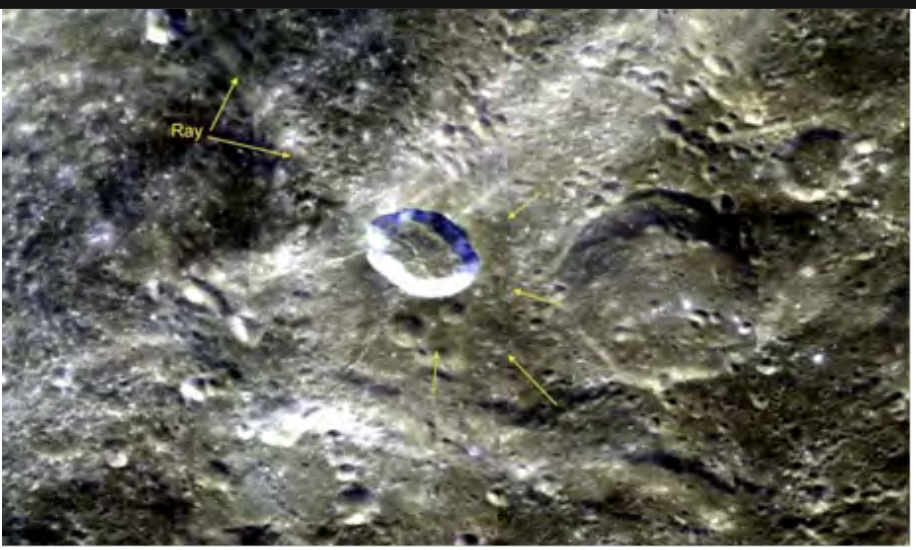

Fig.5 Clementine UVVIS Multispectral Mosaic of Adams B (RGB bands, R 1000 nm, G 900 nm, B 415 nm) showing possible impact melt deposits indicated by arrows. Note the ray to the north-west.

Returning to Fig.1, it is possible to see that the ejecta surrounding Adams B is visible to the north and east where it obscures the underlying Petavius secondaries, and to the south where we see Filaments 1 and 4. Ejecta appears less well developed to the west, but is however represented by a bright ray projecting towards the north-west. This asymmetry may provide evidence of oblique impact with ejecta enhanced cross-range in the form of 'butterfly wing' type deposits (represented by the hummocky deposits to the north) and downrange towards the crater Adams. The ray to the north-west may therefore be an example of an up-range plume, examples of which have been noted extending into the Zone of Avoidance in other oblique impact craters (Bell and Schultz, 2012).

The Clementine Multispectral image shown in Fig.5 indicates the presence of darker impact melt deposits outside the rim of Adams B, whilst Fig.6, a Clementine Ratio Map of the same area shows impact melt rich deposits on the crater floor and surrounding the south-eastern part of the crater. The LRO Quickmap images of this area also reveal a number of small impact melt pools within hollows of the hummocky terrain just outside the north-eastern rim as shown in Fig.7. This distribution of ejecta to the north, south and south-east, combined with the concentration of impact melt to the south-east suggest a probable impactor trajectory from the north-west. This is consistent with the observation of Osinski, et.al (2011) that impact melt beyond crater rims is preferentially concentrated in the downrange direction.

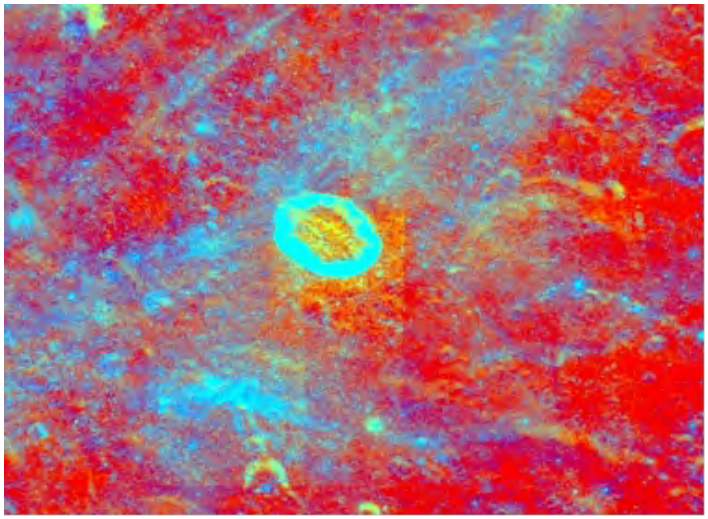

Fig.6
Clementine UV-VIS Ration Map image of Adams B(RGB bands R 750/415nm, G 750/950nm, B 414/750nm) showing impact melt rich deposits as yellow.

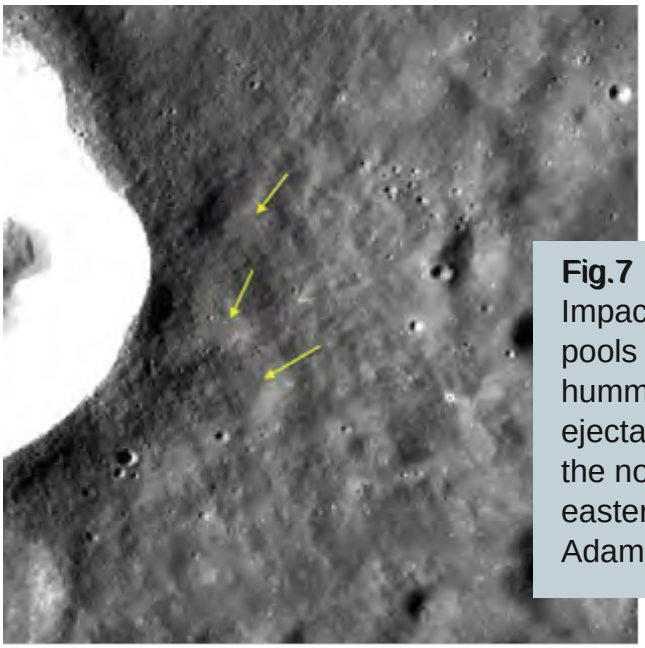

Fig.7
Impact melt pools in hummocky ejecta outside the north-eastern rim of Adams B

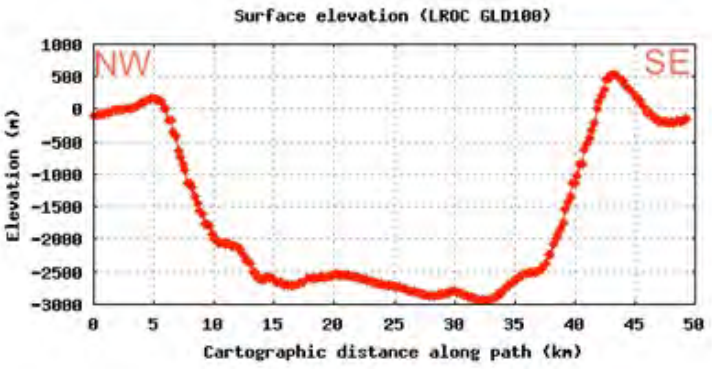

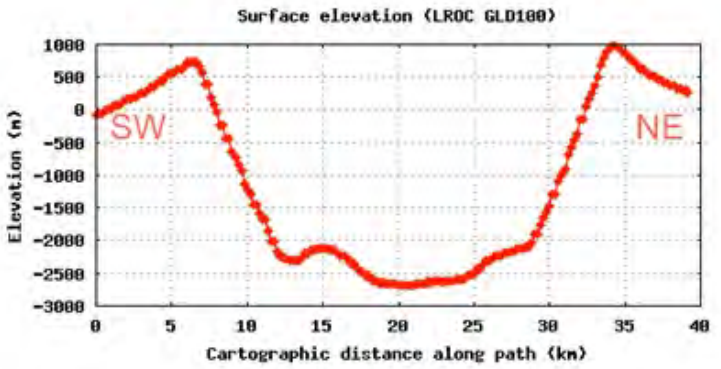

Fig.8
LRO Surface Elevation Profile for Adams B, showing on left the profile from north-west to south-east and the right the profile from south-west to north-east.

The LRO Surface Elevation Profile for Adams B however contradicts this hypothesis to some degree. Very low angle impacts produce elongate craters with a 'saddle shaped' profile, where the down-range rim is lower than the up-range rim, and the height of the rims parallel to the crater long axis are higher than both the former (Forsberg et.al, 1998). Messier is a fine example of this morphology. Fig.8 shows that the lowest section of rim is in fact to the north-west the proposed up-range direction, a fact inconsistent with the usual observations regarding low angle impacts.

This anomaly is clearly seen in the LRO 3D Ground View shown in Fig 9, which shows that the north-western rim of crater A is lower than that of the south-eastern rim of crater C. In between, the parallel walls of crater B are higher still, retaining an overall saddle shaped profile. This anomalous profile with the proposed up-range rim being lower than the down-range one could be a result of the fact that this is not simply a low angle impact (such as that seen in Messier) but a low angle multiple impact, where several impactors of differing size interacted to produce the final crater.

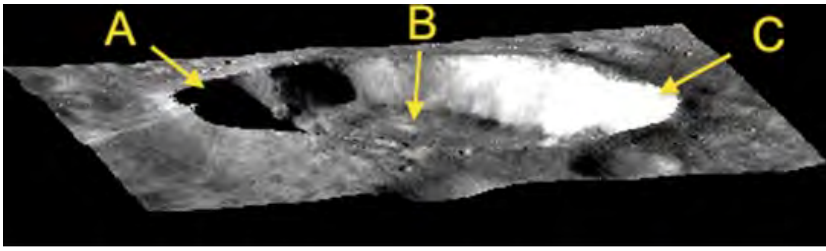

Fig 9
LRO 3D Ground View of Adams B, showing proposed craters A, B and C and showing the differing rim heights.

The interior of Adams B is dominated by fresh impact melt deposits and considerable evidence of wall slumping. Craters A, B and C have floors of differing appearance and form. Crater A, appears to have a roughly semi-circular floor perched at a higher elevation than the floor of crater B as shown in Fig.10. The floor of A appears to have a veneer of impact melt which is exposed as a blocky layer where the floor of A has partially slumped downwards into crater B. To the north of this slumped section the floor of A is intact and preserves a ridge like structure that separates the floor of crater A from that of B. This small northern section may represent a ridge that was initially continuous and separated A from B. Oberbeck (1973) noted that simultaneous closely spaced craters exhibited a septum on the floor separating the individual craters from each other. The ridge seen partially preserved here may represent such a septum. The floor of crater C is also elevated above the floor of B, and again is coated in impact melt deposits of quite a hummocky nature. The observation that the floors of A and C are elevated above that of B is consistent with their being formed by smaller impactors which did not excavate their transient cavities as deeply as the larger B.

The floor of B is elongate along the north-west to south-east axis supporting an oblique impact hypothesis. Running along this axis is a series of low rounded hills which may represent a partially exposed central ridge, which replaces the central peak of higher angle impacts (Fig.11).

There is no indication of this ridge within craters A and C. Extensive impact melt ponds are also evident, with flow channels indicating movement of fluid melt, possibly following displacement by extensive wall slumping into the still molten interior. This can be seen to have occurred below the northern rim, where the slump deposits are coated in a veneer of impact melt, revealed by extensive cooling cracks. The wall slumps themselves are sculpted into a series of linear ridges parallel to the crater walls, possibly indicating multiple phases of collapse. The interior of this crater therefore supports the oblique multiple impact hypothesis, with the distinct crater floors in A, B and C indicating multiple impactors, and the line of central ridge hills the oblique nature of the impact.

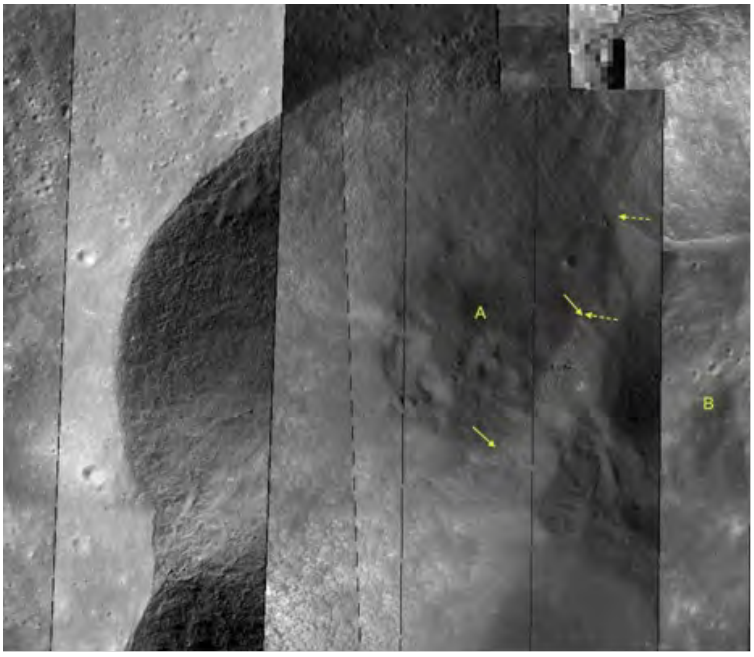

Fig.10
Floor of crater A, showing impact melt floor exposed as rubbly layer (between solid arrows) where the floor has slumped downwards into B. To the north, an intact section of the floor preserves a ridge like structure (between dashed arrows).

Discussion.

Adams B appears to be an unusual crater in that it exhibits features characteristic of both multiple and oblique impacts. Its outline (planform) is suggestive of at least three overlapping craters lining up on a north-west to south-east axis. The central crater (B) appears to be the largest and shows a distinctly elongate in outline, with its northern and southern rim walls being almost parallel. It is possible that the orientation of these walls owes something to tectonic control as they appear parallel to Rimae Hase to the west, it is however more likely that they owe their form to their origin in an oblique impact. The the rims of the smaller crater elements A and C are continuous with that of B indicating a shared origin, whilst their elevated floors relative to B is evidence of their excavation by separate impactors creating their own transient cavity.

The filamentous rays originating along the souther rim at the junctions of the three sub-unit craters (Filaments 1 and 4) are strong evidence of the simultaneity of the impact processes, such rays being diagnostic of this type of impact process. To the north this configuration of rays is obscured by extensive deposits of ejecta which appears to be multi phased, with an earlier deposit dominated by ridges and crater chains overlain by later hummocky deposits. This ejecta appears to form a 'butterfly wing' distribution diagnostic of oblique impacts. The impact melt distribution towards the south-east indicates a projectile trajectory from the north-west. The ray noted as extending to the north-west may represent an up-range plume which crosses a Zone of Avoidance, a further indication of oblique impact processes.

Wood (2012) comments on the bright ray to the north of Adams B, likening it to a 'butterfly wing' from an oblique impact, and draws attention to the absence of any similar ray to the south. The observations outlined above would tend to support his assessment that this crater is the result of an oblique impact. In addition the asymmetry in type and extent of the ejecta described above would be consistent with the ray being prominent to the north, but not the south. Fig.12 illustrates the distribution of bright ray material associated with Adams B, and it is apparent that to the south, bright material appears to be concentrated within proximity of Filaments 1 and 4, but does not extend significantly beyond. This asymmetry may have its origin in the impact dynamics which resulted in filaments being developed to the south, and a butterfly pattern to the north, a hybrid combination of low angle and multiple impact features.

Fig.12
Clementine Basemap image of Adams B showing bright ray distribution.

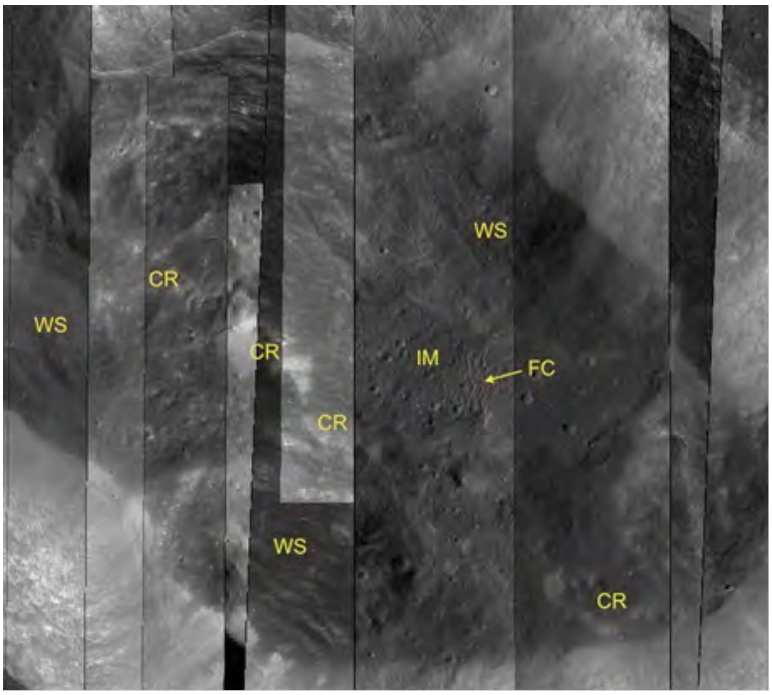

Fig.11
Floor of Adams B showing Impact Melt (IM) with flow channels (FC). This flow may have been caused by displacement of melt by wall slumping (WS) from the northern rim. A line of rounded hills may represent a central uplift ridge (CR).

References

Bell, S.B and Schultz, P.H. (2012) Detection of a Radar Signature of the Uprange Plume in Fresh Oblique Lunar Craters. 43rd Lunar and Planetary Science Conference, held March 19–23, 2012 at The Woodlands, Texas. LPI Contribution No. 1659, id.2824

Bottke, W.F, Love, S.G, Tytell, D and Glotch, T. 2000. Interpreting the Elliptical Crater Populations on Mars,Venus, and the Moon.Icarus 145, 108–121

Bottke, W.F and Melosh, H.J. 1996. Binary Asteroids and the formation of Doublet Craters. Icarus, Volume 124, Issue 2, pp. 372-391

Forsberg, N. K., Herrick, R. R., Bussey, B. 1998. The Effects of Impact Angle on the Shape of Lunar Craters. 29th Annual Lunar and Planetary Science Conference, March16-20, 1998, Houston, TX, abstract no. 1691.

Gault, D. E. & Wedekind, J. A, 1978. Experimental Studies of Oblique Impact, LUNAR AND PLANETARY SCIENCE IX, PP. 374-376.

Oberbeck, V.R and Morrison, R.H 1973. On the formation of the lunar herringbone pattern. Proceedings of the Lunar Science Conference, vol. 4, p.107

Oberbeck, V.R and Morrison, R.H 1974. Laboratory Simulation of the Herringbone Pattern Associated with Lunar Secondary Crater Chains. The Moon, Volume 9, Issue 3-4, pp. 415-455

Oberbeck, V. R, 1973. Simultaneous Impact and Lunar Craters.The Moon, Volume 6, Issue 1-2, pp. 83-92

Osinski, G.R, Tornabene, L.L and Grieve, R.A.F, 2011. Impact ejecta emplacement on terrestrial planets. Earth and Planetary Science Letters 310 (2011) 167–181

Wood, C. 2012. The Adams Family, LPOD Lunar Picture of the Day, December 4th 2012. (https://lpod.wikispaces.com/December+4,+2012)

Acknowledgements

LROC images and topographic charts reproduced by courtesy of the LROC Website at http://lroc.sese.asu.edu/index.html, School of Earth and Space Exploration, University of Arizona.

Clementine Multispectral Images courtesy of the USGS PSD Imaging Node at http://www.mapaplanet.org/

Selenology Today

TARGETS TO EXPLORE

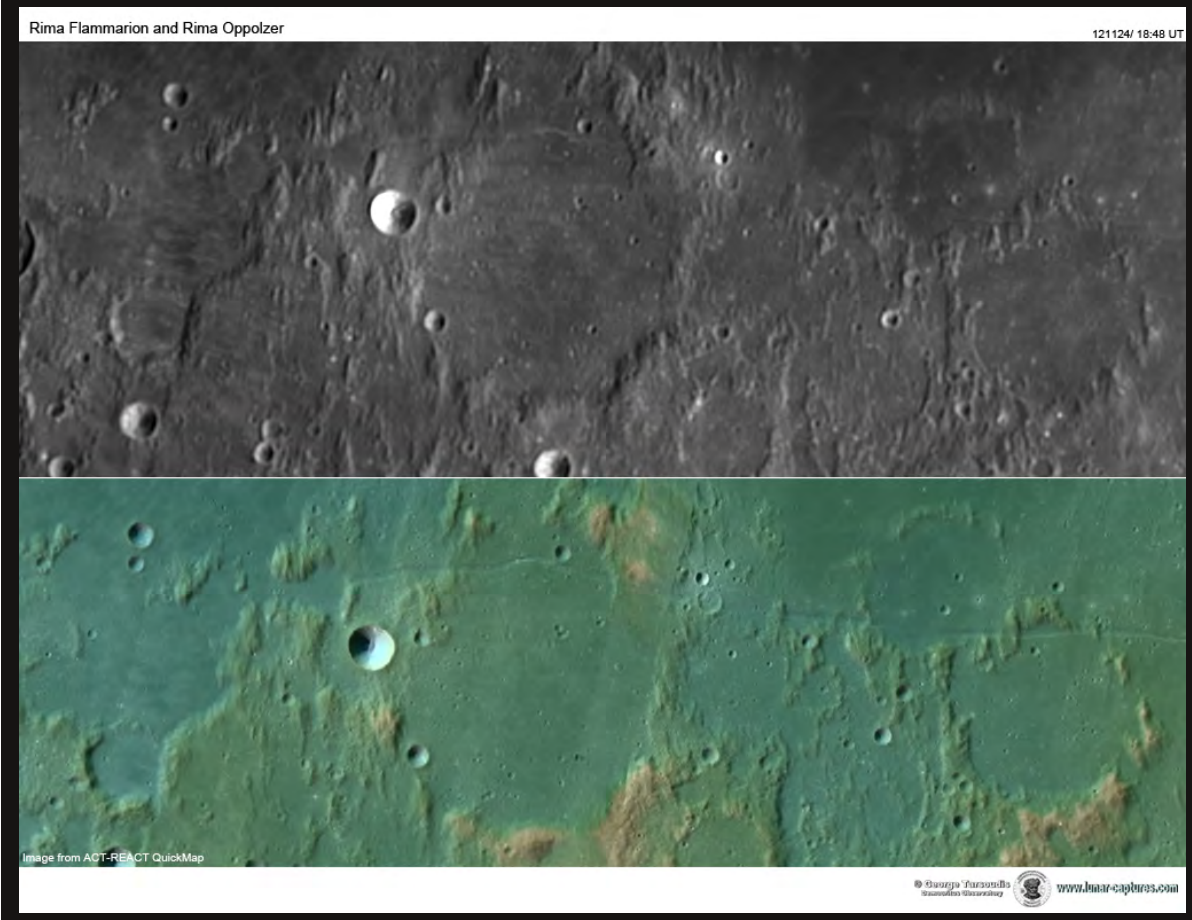

Rima Oppolzer
and Rima Flammarion

Equipment
Telescope 10 inch @f/6.3
Camera Unibrain fire-i 785
Filters Red
Barlow 3X

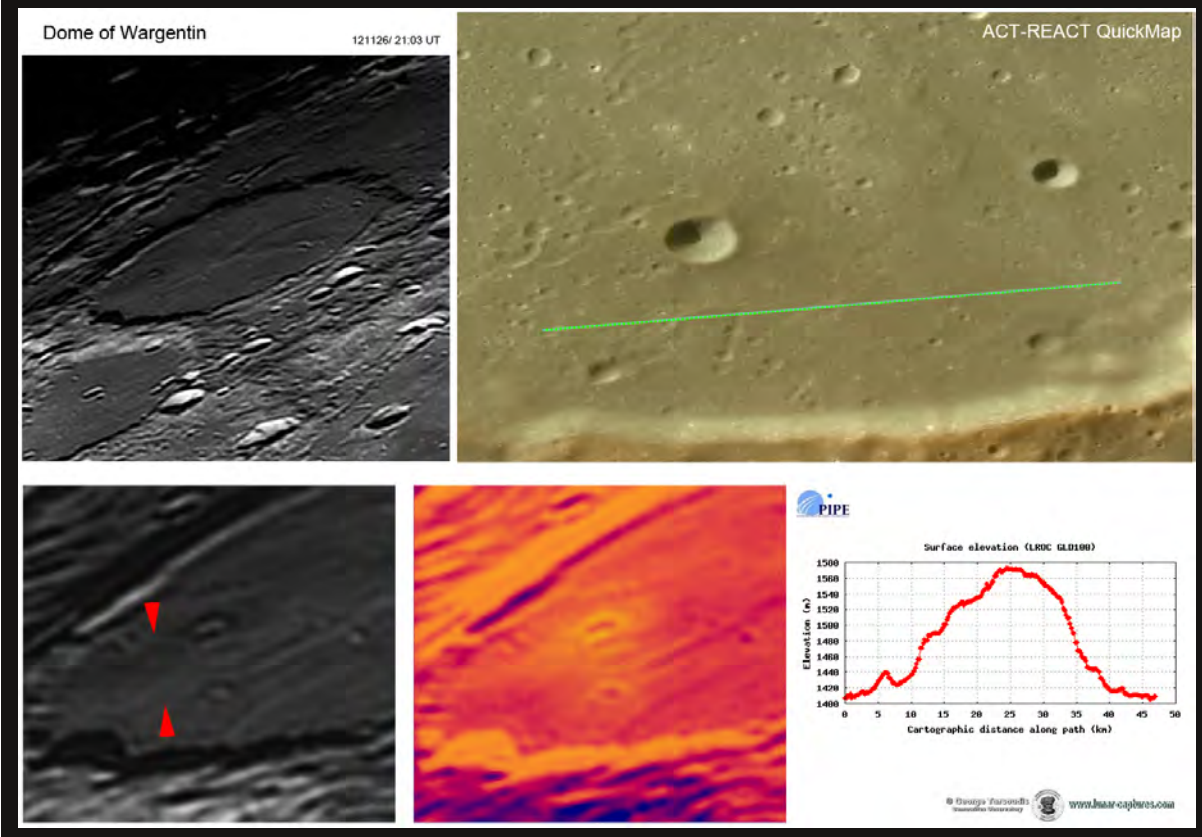

Dome Wargentin, you will need to do more study.

Equipment
Telescope 10 inch @f/6.3
Camera Unibrain fire-i 785
Filters Red
Barlow 3X